Chapter - 6

Effect of Growth under Electric Field on Structural, Electrical and Optical Properties of L-Cysteine and L-Arginine doped Potassium Dihydrogen Phosphate (KDP) crystals.

Chapter-6: Effect of Growth under Electric Field on Structural, Electrical and Optical Properties of L-Cysteine and L-Arginine Doped Potassium Dihydrogen Phosphate (KDP) Crystals

1. Introduction:

Potassium Dihydrogen Phosphate (KDP) crystals have an immense worldwide demand because they are useful for second, third, and fourth harmonic generators for lasers. Due to its potential uses in electro-optics, acousto-optics, photonics, and other fields, the ferroelectric KDP crystal has played a significant role in device innovations. Certain properties of the KDP crystal, such as ferroelectricity, good piezoelectricity, and optical homogeneity, make it appropriate for second harmonic generation (SHG) devices [1]. This is so since KDP is an optically transparent crystal and exhibits good non-linear optical and electro-optical properties [2]. KDP single crystals are paraelectric at room temperature, with good structural efficiency, a high non-linear optical coefficient, and good mechanical properties [3]. On the other hand, organic materials have several interesting features that could be used in non-linear optical (NLO) applications. Because of this, the semi-organic class of materials has been acquiring an interest in the recent past because of their potential use in NLO applications. The most common type of hybrid NLO material is semi-organic compounds [4]. NLO crystals are used extensively in lasers and, in particular, in Pockel's cells. In recent years, there has been a tremendous increase in scientific interest in water-soluble crystals that contain complex organic compounds [5]. In recent years, the investigation of non-linear optical characteristics of various organic, inorganic, and semi-organic materials has attracted considerable interest. New techniques are evolving, and existing ones are being modified to produce larger size crystals, with better perfection, and, in certain cases, with modified habits to meet needs in various fields of science and technology.

For appropriate device-oriented research and applications, crystal habit modification is frequently a requirement. To meet such requirements, crystal growth conditions and additives in the crystal typically prove highly effective. As a result, appropriate habit modification while simultaneously improving crystal growth rate may become quite desirable for a crystal growth technique. The width of the metastable zone, the supersaturated region, and the solution's stability all play a role in crystal growth in the solution. With an increase in the width of the metastable zone, the solution stability improves and for a high growth rate, this dependence is very important. In the supersaturated region, the metastable zone width plays a crucial role and

accordingly, various procedures and additives are adapted for enhancing the metastable zone breadth and the growth rate. The width of the metastable zone can be affected by impurities in the solution. Sometimes the amount of impurity added, and nature of solution become deciding factors for the width of a metastable region. Some additives can induce secondary nucleation, which can lead to a reduction in the metastable zone region.

Chelating agents are used as additives for the rapid growth of KDP crystals. Some chelating agents may enhance chemical activity, while others suppress it depending on the bond formation of additives with KDP. The most typical habit of KDP crystal is the combination of the tetragonal prism and the pyramid with (100) and (101) planes, respectively [7]. Additives or dopants play a major role in determining the width of the metastable zone of a solution. Habit change can take in two forms: either new 'h k l' forms or changes in the relative development of existing 'h k l' occur. Some faces of a doped crystal develop faster than those of a pure crystal, which can be accomplished using appropriate dopants or additives. The presence of additives or dopants alters the optical properties as well as the structural quality of crystals. Under the influence of an applied electric field, we have grown pure KDP, L-Cysteine doped KDP, and L-Arginine doped KDP crystals under an applied d. c electric field too. Electrical characteristics, optical properties, second harmonic generation efficiency and other characteristics of KDP have been reported to be enhanced with the doping of L-Cysteine and L-Arginine in several investigations [8,9]. Aside from doping, there are also plenty of other factors that can influence crystal growth. Because KDP is a non-centrosymmetric crystal, studying its crystal formation under a d. c electric field would be interesting. There hasn't been a study like this found in the literature to the best of our knowledge. The results of crystal growth in the presence and absence of an externally applied electric field are presented and discussed in the following sections.

2. Experimental details:

AR grade potassium dihydrogen phosphate (KDP), L-Cysteine and L-arginine were used to grow the crystals. 1 mol% and 2 mol% of L-Cysteine and L-Arginine each were mixed with the solution of KDP. The solution was stirred for 3-4 hours until it became homogeneous. The solutions of pure KDP, L-Cysteine (1 mol% and 2 mol%) doped KDP and L-Arginine (1 mol% and 2 mol%) doped KDP were placed into five separate beakers covered with perforated paper sheets to allow slow evaporation. At the same time, the other five beakers were kept in a constant electric field of 320 V/cm. Two parallel metal plates were attached to a non-conducting

base and coupled to a constant d. c voltage supply to create the field. The arrangement was held at room temperature (32°C) and isolated from transient disturbance.

After 28-30 days, transparent, high-quality crystals were harvested. The crystals formed in the presence of the electric field were noticeably more transparent than those grown in the absence of one. This could be related to the effect of the externally imposed electric field on the polar molecules in the solution, which causes the latter to take longer to reach supersaturation, resulting in superior crystal quality than those produced without the electric field. It was observed that sizable crystals could be obtained from the solution kept in an electric field after a growth period of 10-15 days more than that of crystals grown without the electric field. The doped crystals display elongation along a certain axis (c-axis), as seen in figure 2. The doped crystals grown in the presence of an electric field was found to have a greater degree of elongation. It was found that L-Cysteine doped KDP crystals growing in the presence of an electric field had a slight habit modification. In contrast, significant habit modification is seen in the L-Arginine doped KDP crystals, as seen in figure 2. The fully or partially forced alignment of the dipoles in the crystal along the direction of the d. c. electric field applied during crystal growth may cause habit modification. To perform paper chromatography, the crystals were dissolved in de-ionized water. Purple colouring was observed using ninhydrin ($C_9H_4O_3$), indicating the presence of amino acid in the doped crystals.

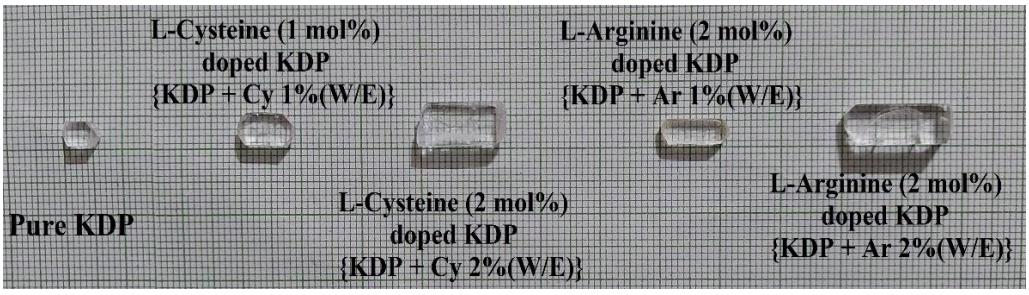

Figure 1. Pure KDP, L-Cysteine (1 mol% and 2 mol%) doped KDP and L-Arginine (1 mol% and 2 mol%) doped KDP crystals grown in the presence of an electric field

3. Results and Discussion:

3.1 Powder X-ray Diffraction (XRD) Analysis:

The XRD plots for pure KDP, L-Cysteine (1 mol% and 2 mol%) doped KDP and L-Arginine (1 mol% and 2 mol%) doped KDP crystals produced under an applied electric field, respectively, are shown in figures 3(a-b). There is no phase transition of the crystal due to doping and growth under an electric field, as shown in the plots. Pure and doped KDP crystals have sharp diffraction peaks, indicating excellent crystalline perfection [10]. With the help of

FullProf Suite software, the XRD peaks were analyzed and indexed. It can be shown that neither doping nor applying an electric field during crystal growth produced any modifications in the peaks. As shown in table 1, the inter-planar spacings and lattice parameters evaluated using this software and the cell volume do not indicate any significant change. These structural results are in perfect accordance with pure KDP lattice characteristics previously published.

As a result, even after doping with L-Cysteine and L-Arginine, KDP retains its single-phase structure. According to the calculated lattice parameters, it seems that the dopants L-Cysteine and L-Arginine are well accommodated in the crystal lattice. However, all the doped crystals appear to have minor local distortions [11]. The overall growth crusade in steps may be blocked or be erratic due to impurities attaching to the crystal lattice. In contrast, other species may assemble rapidly across the same surface in the same direction. This occurs when doped crystals are grown in the presence of an electric field. The above phenomenon occurs when the average distance between the impurities is less than two times the radius of the two-dimensional critical nucleus [12]. Due to variations in growth kinetics, this could eventually result in a change in the crystalline phase habit. Therefore, accommodation of L-Cysteine and L-Arginine in the lattice of KDP crystal must exert less strain when grown in the presence of an electric field.

Compared to crystals grown in the absence of an electric field, crystals grown in the presence of an electric field exhibit less strain, as indicated in table 2. The incorporation of dopants causes the shifting of specific prominent peaks, as shown in figure 3(c). However, in terms of the instrument resolution, this shift may be regarded as insignificant. The strain on the lattice induced by amino acid absorption in the KDP lattice could cause this shift.

Table 1. Unit cell parameters of pure and doped KDP crystals

Crystals	a (Å)	b (Å)	c (Å)	Volume	Symmetry
Reported KDP	7.448	7.448	6.977	387.033	Tetragonal
Pure KDP W/E	7.453	7.453	6.975	387.456	
KDP + Cy 1% W/E	7.453	7.453	6.974	387.484	
KDP + Cy 2% W/E	7.456	7.456	6.972	387.907	
KDP + Ar 1% W/E	7.452	7.452	6.974	387.554	
KDP + Ar 2% W/E	7.453	7.453	6.975	387.616	

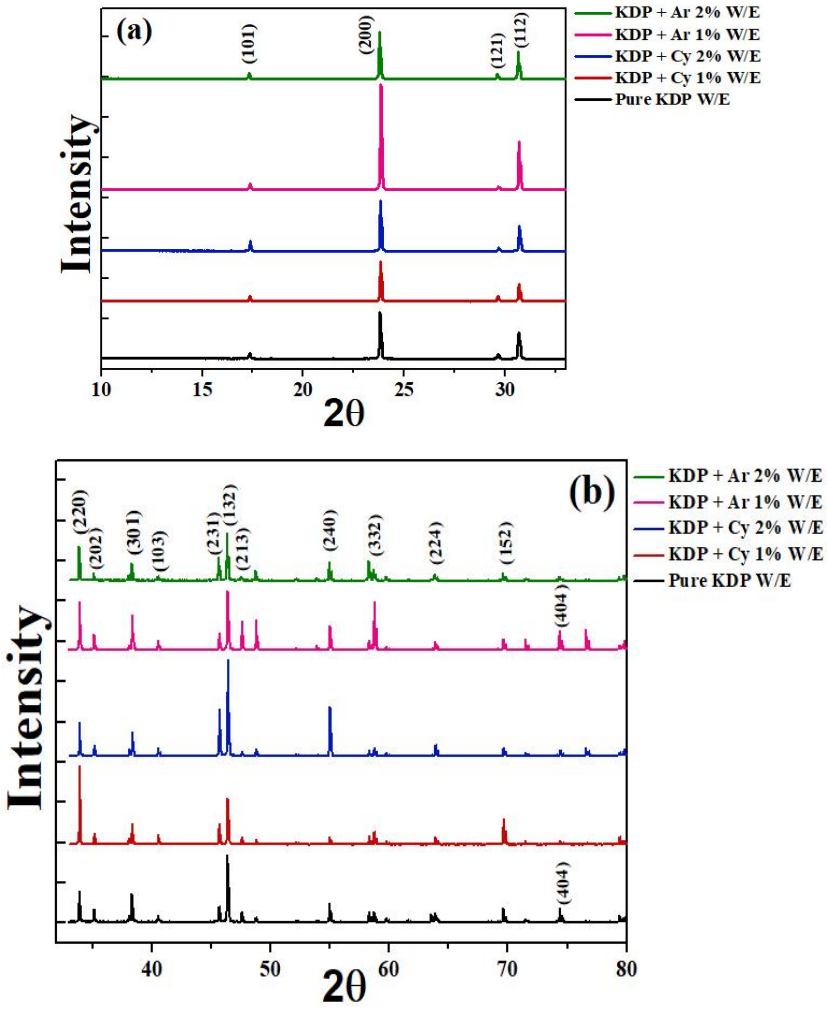

Figures 3(a-b). XRD plots of pure, L-Cysteine (1 mol% and 2 mol%) and L-Arginine (1 mol% and 2 mol%) doped KDP crystals

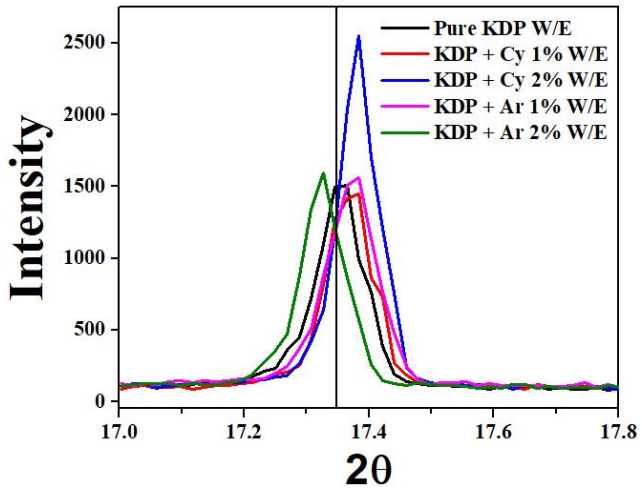

Figure 3(c). Peak (101) shifting of pure and doped KDP crystals grown in the presence of electric field

Table 2. Variation in structural parameters of pure and doped KDP crystals grown in presence of an electric field

Sample	FWHM	2θ	Crystallite Size t (nm)	Strain ε ($lin^{-2}\ m^{-4}$)	Dislocation Density δ ($lin\ m^{-4}$)
Pure KDP W/E	0.0925	17.35	1.51	2.29E-02	3.03E-02
	0.0992	23.81	1.42	2.43E-02	3.43E-02
KDP + Cy 1% W/E	0.0883	17.36	1.58	2.18E-02	2.77E-02
	0.0953	23.83	1.48	2.33E-02	3.16E-02
KDP + Cy 2% W/E	0.0781	17.38	1.79	1.93E-02	2.16E-02
	0.0948	23.83	1.49	2.32E-02	3.12E-02
KDP + Ar 1% W/E	0.0961	17.37	1.45	2.38E-02	3.28E-02
	0.0931	23.85	1.52	2.28E-02	3.02E-02
KDP + Ar 2% W/E	0.0860	17.32	1.63	2.13E-02	2.63E-02
	0.0965	23.78	1.46	2.36E-02	3.24E-02

3.2 Dielectric Analysis:

An anisotropic ferroelectric crystal contains spontaneously polarised regions that explain its electrical and other properties. One of the remarkable phenomena emerging from crystal anisotropy is the piezoelectric effect. The effect is the occurrence of electrical polarization generated by mechanical stress, while the converse effect is deformation caused by an applied electric field. Ionic polarization occurs due to relative ion displacement and is most commonly seen in crystals with a strong ionic bond. However, it should be noted that polarization due to electron dislocation of ions can occur alongside ion-dislocation polarization in such crystals. Ionic conductivity is favoured by direct dielectric crystals (intrinsic and impurity) [13].

Electrical conductivity studies on various ionic crystals reveal that the primary current transporters are the ions with the smallest size and equivalent charge or those with comparable sizes but lower charge. For example, the major current carriers in PbCl are Cl^-, while the principal charge carriers in NaCl are Na^+. Some crystals, such as PbI_2, have electrical conductivity due to ions of both signs. Charge carrier concentration is also influenced by temperature. A rise in temperature in some crystals can result in the production of carriers of both signs in place of pre-existing carriers of the same sign. The charge carriers in NaCl and NaF are Na^+ ions but, at 600°C, Cl^- and F^- also play a minor role in charge transport [13]. In strong fields, the electronic conductivity of many dielectric crystals is overlaid over the ionic conductivity. Quartz, rock salt and other minerals exhibit this effect. For example, in mica, the electronic conductivity prevails at low temperatures, whereas ionic conductivity dominates at

high temperatures, even in the presence of weak fields. Electrical conductivity in ionic crystals is caused by the movement of the crystal lattice ions, and at high temperatures, this conductivity contributes most prominently.

On the other hand, we can say that electrical conductivity in ionic crystals at low temperatures is caused by the motion of relatively weakly fixed impurity ions. Both lattice ions and weakly bound impurity ions cause this conductivity [13]. Dipolar, ionic, electronic and space charge polarizations contribute to the dielectric constant of materials at lower frequencies. However, these polarizations lose their relevance at high frequencies. The low value of dielectric constant allows for lower power consumption [14]. With increasing temperature, the dielectric constant and dielectric loss of pure and doped KDP crystals grown in the presence of an electric field increases. The amount of electrically active defects in a good NLO material is a crucial aspect. The lower the dielectric constant, the lesser the electrically active defects and crystal quality will also be better [15]. Crystals that have fewer defects are more suitable for NLO applications. These features are ideal to produce electro-optic and NLO devices. Protonic conductors are used in fuel cells, high energy density batteries, sensors and other applications. Ionic, electronic, or both the conductivities can be found in dielectrics. The dielectric constant and dielectric loss of L-Cysteine (1 mol% and 2 mol%) doped KDP and L-Arginine (1 mol% and 2 mol%) doped KDP crystals are given in figures 4(a-d) and figures 5(a-d). The inset figures correspond to pure KDP crystal grown under an applied electric field.

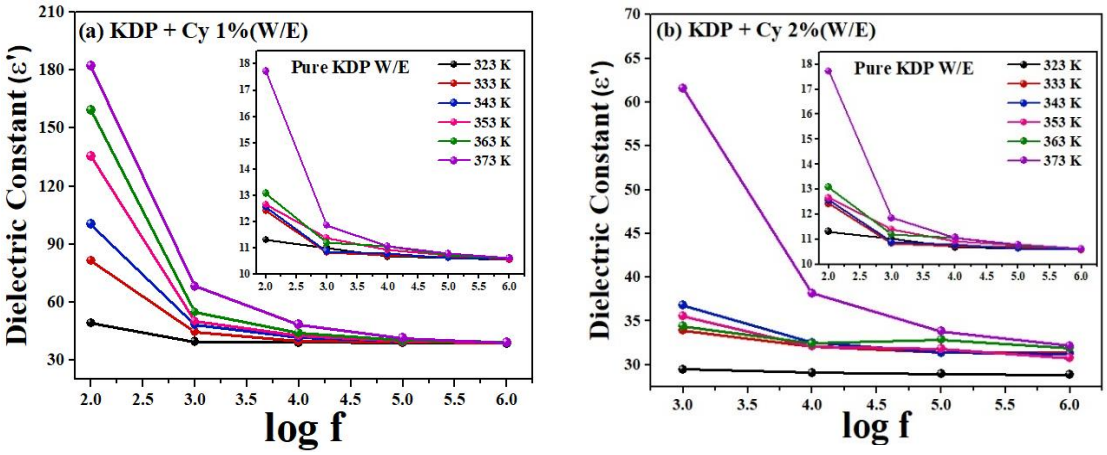

Figures 4. (a) The dielectric constant of L-Cysteine (1 mol%) doped KDP crystals and **(b)** The dielectric constant of L-Cysteine (2 mol%) doped KDP crystals

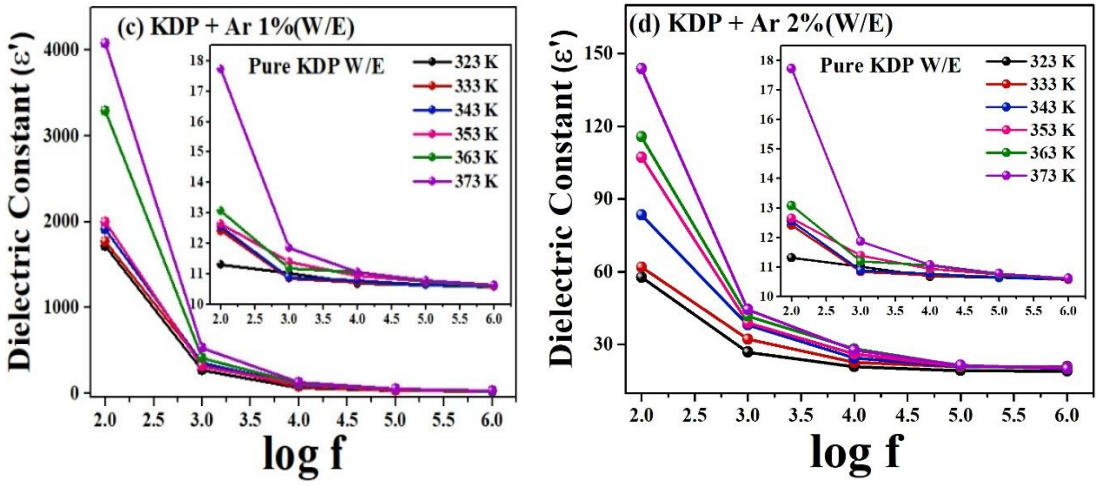

Figures 4. (c) The dielectric constant of L-Arginine (1 mol%) doped KDP crystals and **(d)** The dielectric constant of L-Arginine (2 mol%) doped KDP

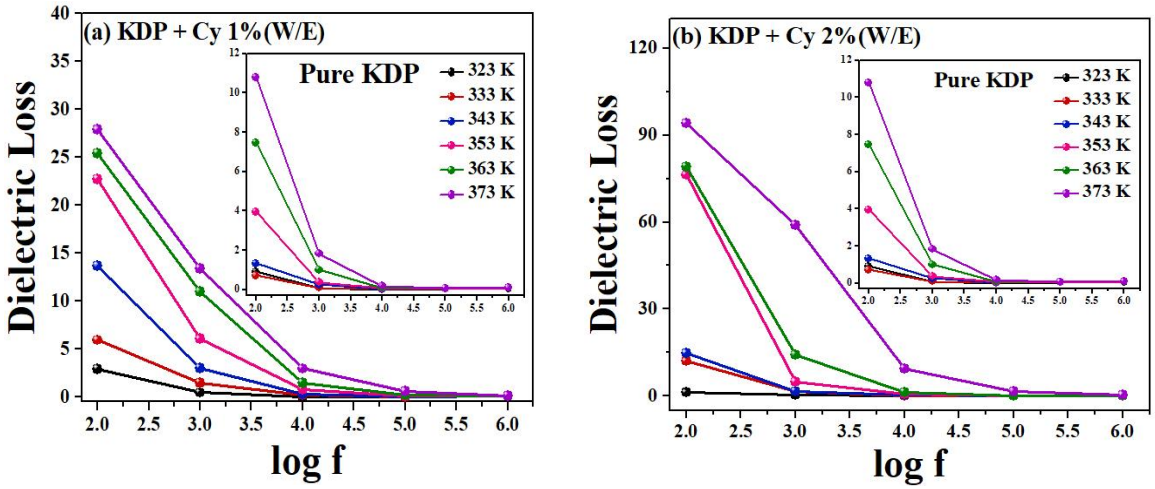

Figures 5. (a) The dielectric loss of L-Cysteine (1 mol%) doped KDP crystals and **(b)** The dielectric loss of L-Cysteine (2 mol%) doped KDP

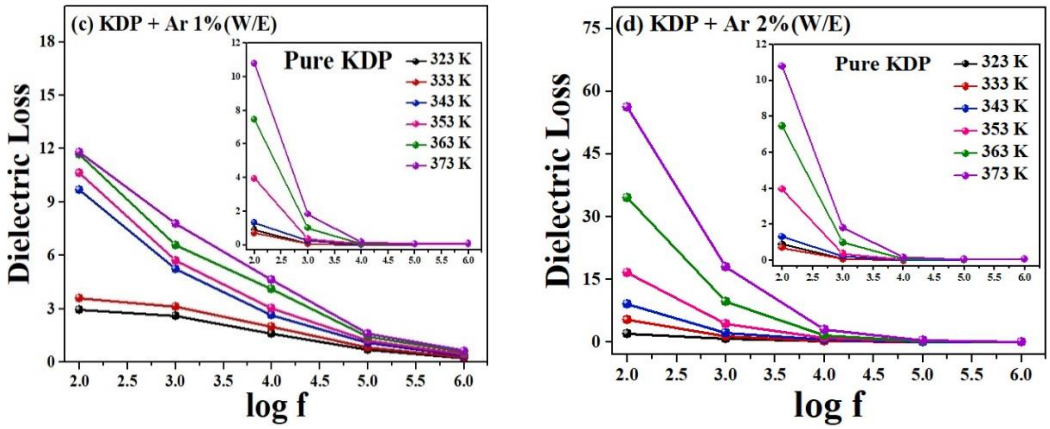

Figures 5. (c) The dielectric loss of L-Arginine (1 mol%) doped KDP crystals and **(d)** The dielectric loss of L-Arginine (2 mol%) doped KDP crystals

3.2.1 Impedance Spectroscopy:

Figures 6(a-e) show Nyquist plots [real part of complex impedance (Z') against imaginary part of complex impedance (Z'')] of pure, L-Cysteine (1 mol% and 2 mol%) doped KDP and L-Arginine (1 mol% and 2 mol%) doped KDP crystals grown in the presence of an electric field. The motion of charges can be explained in a variety of ways. Dipole re-orientation, space charge formation and charge displacement are among them. A single semicircular arc is observed at each temperature, as shown in the figures. The centre of each semi-circle falls below the real axis (Z') due to the presence of temperature-dependent multi-relaxation processes. These graphs show the bulk ionic conductivity of the crystals at various temperatures. This suggests that the crystals have non-Debye behaviour. A tail (or spike) is observed at lower frequencies, and the polarization of the electrode/electrolyte could be the cause of this. By fitting the semi-circles of the Nyquist plot, the values of bulk resistance, capacitance and relaxation time were calculated and are listed in tables 3 and 4.

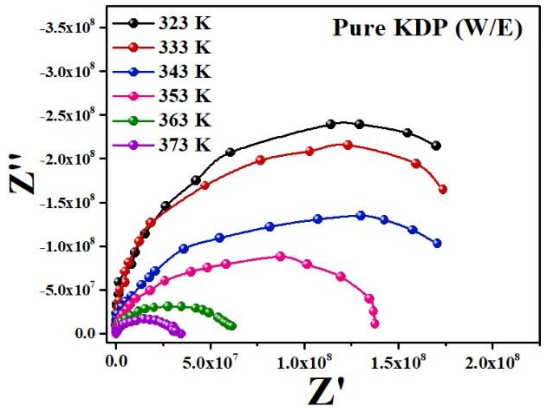

Figure 6(a). Nyquist plot of pure KDP crystal

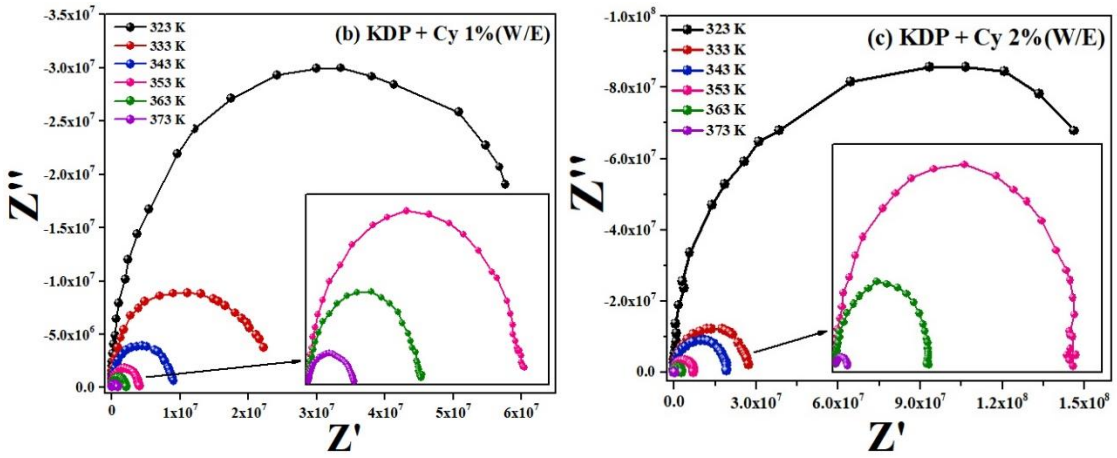

Figures 6. (b) Nyquist plots of L-Cysteine (1 mol%) doped KDP crystals and **(c)** Nyquist plots of L-Cysteine (2 mol%) doped KDP crystals

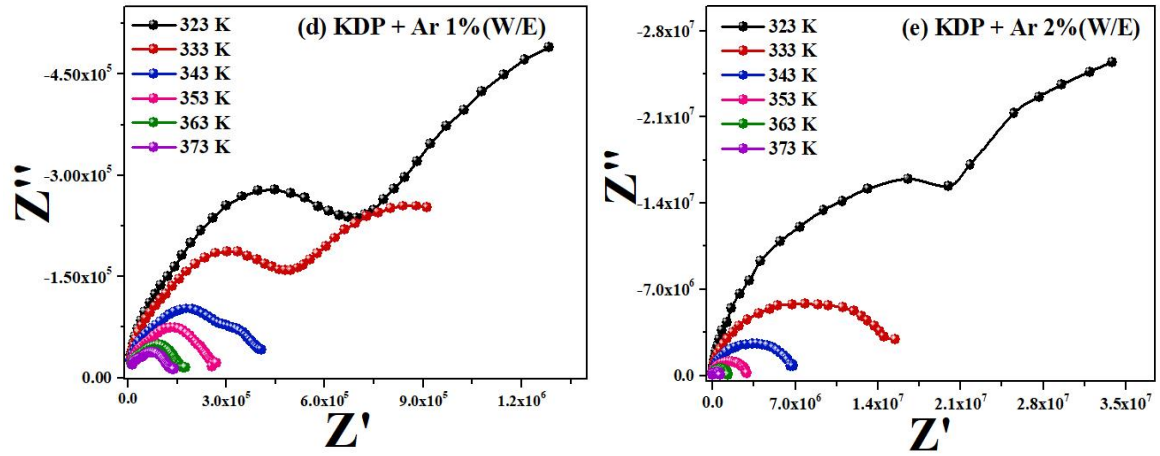

Figures 6. (d) Nyquist plots of L-Arginine (1 mol%) doped KDP crystals and **(e)** Nyquist plots of L-Arginine (2 mol%) doped KDP crystals

From figures 6(d-e), it is observed that there is the formation of a small second semi-circle; however, as the temperature rises, this second semi-circle is shifted to form one semi-circle. It might be possible that L-Arginine doped KDP crystals grown in the presence of the electric field have both the grain resistance and the grain boundary resistance, though only up to 343 K.

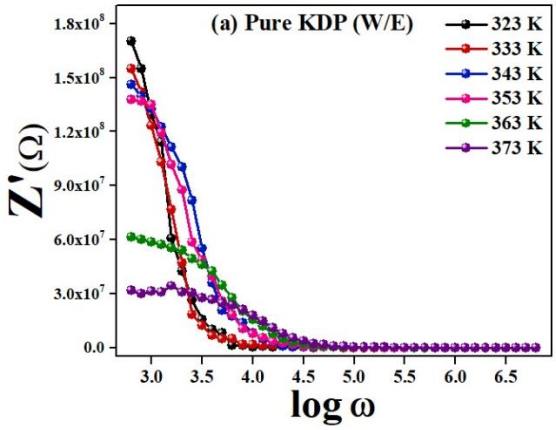

Figure 7 (a). Z' versus log ω of pure KDP crystal

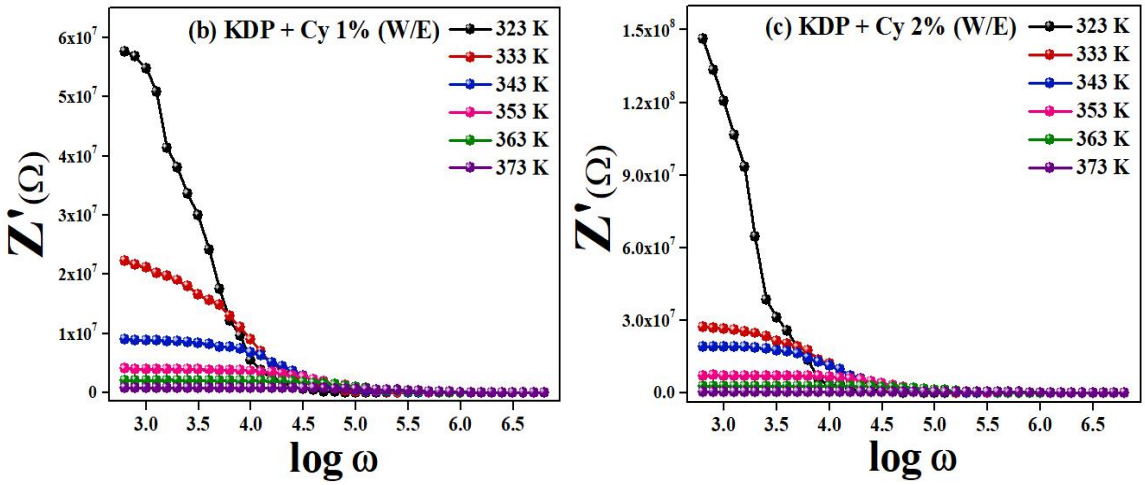

Figures 7. (b) Z' versus log ω of L-Cysteine (1 mol%) doped KDP crystals and **(c)** Z' versus log ω of L-Cysteine (2 mol%) doped KDP crystals

Figures 7(a-e) and 8(a-e) show the correlation between the real (Z') and imaginary (Z'') parts of impedance and frequency at various temperatures. The decrease in the value of Z' with temperature implies that the crystals have a negative temperature coefficient of resistance (NTCR). The magnitude of the real part of the complex impedance (Z') for all the crystals decreases with increasing frequency and temperature, indicating an increase in a. c conductivity, as shown in figures 7(a-e). In addition, as the frequency increases, Z' at all temperatures merges and becomes constant for all crystals, possibly due to space charge discharge [16]. In Z'' versus frequency plots [figures 8(a-e)], the asymmetric broadening of peaks corresponds to a range of relaxation periods, indicating that the material exhibits a temperature-dependent electrical relaxation phenomenon.

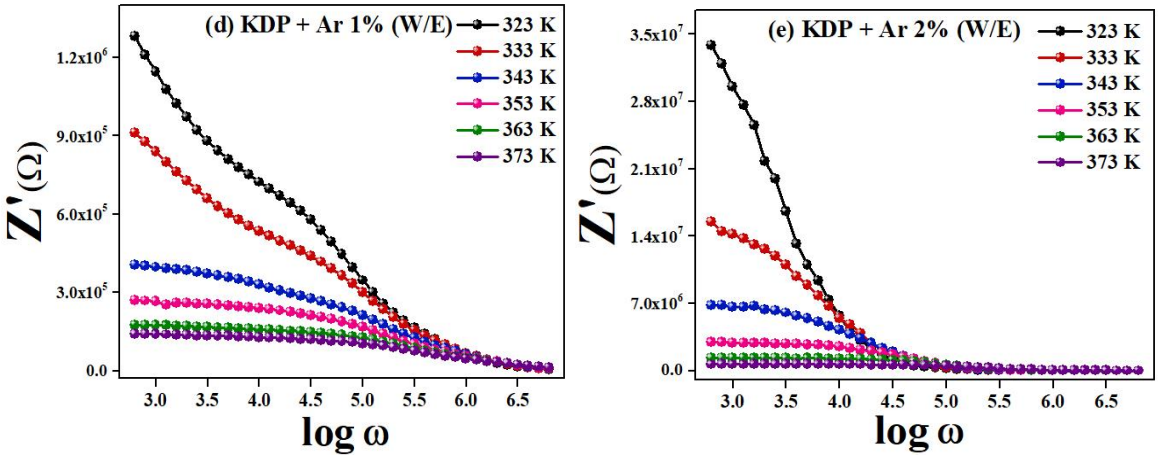

Figure 7. (d) Z' versus log ω of L-Arginine (1 mol%) doped KDP crystals and **(e)** Z' versus log ω of L-Arginine (2 mol%) doped KDP crystals

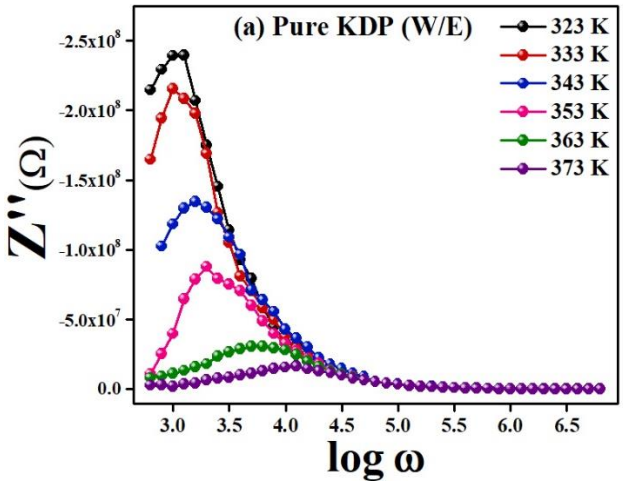

Figure 8(a). Variation in the imaginary part of impedance (Z'') with frequency for pure KDP crystal

Table 3. Nyquist parameters of L-Arginine (1 mol% and 2 mol%) doped KDP crystals

Temperature	KDP + Ar 1% (W/E)			KDP + Ar 2% (W/E)		
	R_g (Ω)	C_g (pF)	τ (μs)	R_g (Ω)	C_g (pF)	τ (μs)
323 K	1.54E+06	10.3406	15.9235	3.34E+07	9.5011	317.71
333 K	6.72E+05	18.8272	12.6485	1.19E+07	13.3766	159.23
343 K	3.91E+05	16.215	6.3392	5.85E+06	13.6480	79.80
353 K	2.90E+05	17.3409	5.0354	2.53E+06	9.9724	25.23
363 K	2.02E+05	19.7541	3.9990	1.23E+06	8.1816	10.04
373 K	1.80E+05	17.6372	3.1771	6.78E+05	7.4270	5.03

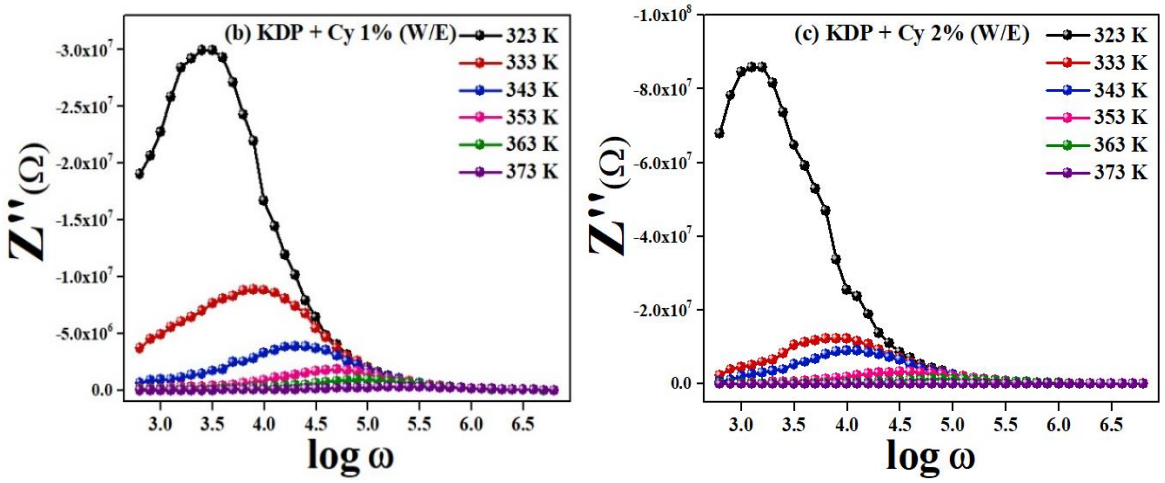

Figures 8. (b) Variation in the imaginary part of impedance (Z'') with frequency for L-Cysteine (1 mol%) doped KDP crystals and **(c)** Variation in the imaginary part of impedance (Z'') with frequency for L-Cysteine (2 mol%) doped KDP crystals

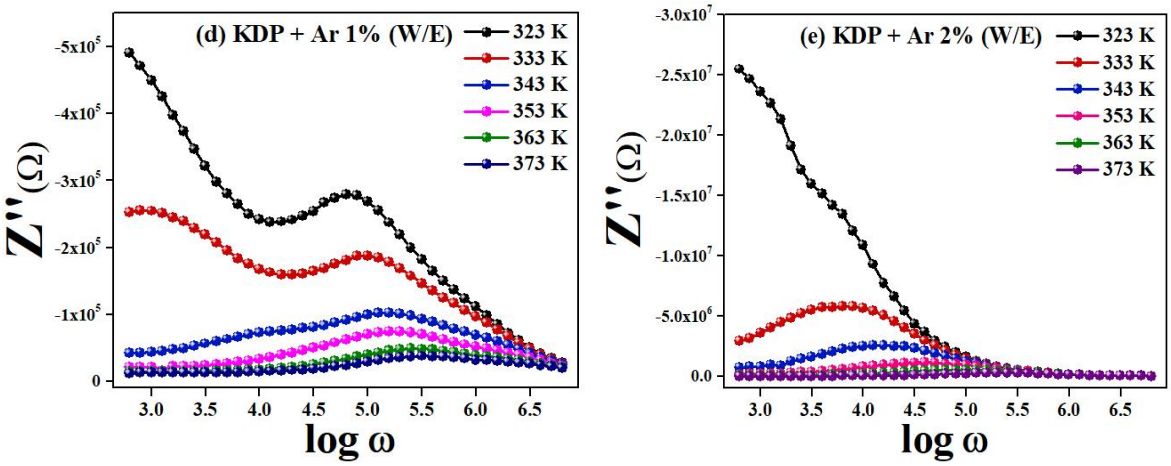

Figures 8. (d) Variation in the imaginary part of impedance (Z'') with frequency for L-Arginine (1 mol%) doped KDP crystals and **(e)** Variation in the imaginary part of impedance (Z'') with frequency for L-Arginine (2 mol%) doped KDP crystals

Table 4. Nyquist parameters of pure and L-Cysteine (1 mol% and 2 mol%) doped KDP crystals

Temerature	KDP (W/E)			KDP + Cy 1% (W/E)			KDP + Cy 2% (W/E)		
	R_g (Ω)	C_g (pF)	τ (ms)	R_g (Ω)	C_g (pF)	τ (ms)	R_g (Ω)	C_g (pF)	τ (ms)
323 K	9.40E+09	0.1068	1.0047	6.08E+07	6.5836	0.3999	1.41E+08	5.6773	0.7980
333 K	3.47E+08	2.2979	0.7980	1.93E+07	6.5482	0.1264	4.08E+07	3.0964	0.1264
343 K	2.23E+08	2.8392	0.6339	7.94E+06	6.3428	0.0503	1.90E+07	4.2080	0.0798
353 K	1.55E+08	3.2543	0.5035	3.86E+06	5.1896	0.0200	7.28E+06	4.3659	0.0317
363 K	6.03E+07	2.6391	0.1592	2.08E+06	6.0816	0.0126	2.80E+06	3.5906	0.0100
373 K	3.28E+07	2.4335	0.0798	7.68E+05	5.2060	0.0039	3.30E+05	3.0436	0.0010

3.2.2 A. C Conductivity Mechanism:

Figures 9(a-e) shows the variation of a. c conductivity with angular frequency, in pure and doped KDP crystals, at different temperatures ranging from 323 K to 373 K. Ionic conductivity can become quite important due to migration or transit of positive or negative ions. Some defects and ions can also be considered basic components required for conduction in ionic crystals. Because KDP crystals are ionic, proton transport occurs within the framework of H-bonds, and this predominant transport mechanism determines the electrical conductivity of these crystals. The conductivity can be explained based on a mixture of impurities present in the network and the formation of defects in the ionic crystals [17]. The two types of defects are: doubly occupied H-bonds and vacant H-bonds.

The H-atom has the ability to form covalent bonds with electronegative atoms, including carbon, oxygen and nitrogen, and can also make extra H-bonds; however, this is a scarce capability. It can also increase the size of its covalency, which has directional qualities [18,19]. In such circumstances, oscillations of the H-atom would presumably cause a shift in its equilibrium position, resulting in proton transport. The H-bond has varying magnitudes along different crystal axes depending on the lattice structure, and proton transport occurs due to this directional property of the H-bond. When L-Arginine and L-Cysteine are doped into KDP, they will accommodate in the crystal lattice of KDP and create L-defects. The proton transport mechanism is primarily responsible for the creation of L-defects [20]. According to Lokshin [21], HPO_4^{2-} is also responsible for forming unoccupied H-bonds (L-defects). KDP is protonic mostly because of the anions [$H_2PO_4^-$ ions] rather than the cations [K^+ ions], with

additional H-bonds formed that enhance proton migration. As a result, as the dopant concentration increases, the conductivity increases as well [22].

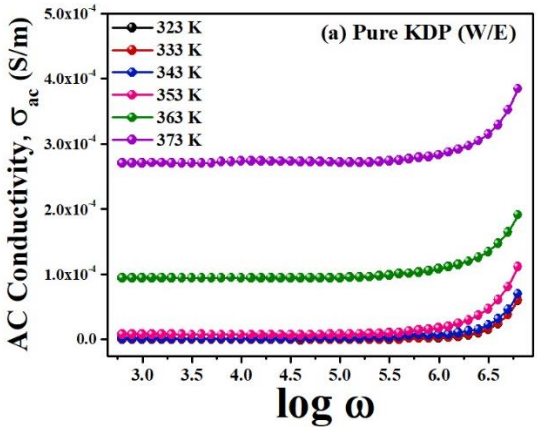

Figure 9(a). A. C Conductivity of pure KDP crystal

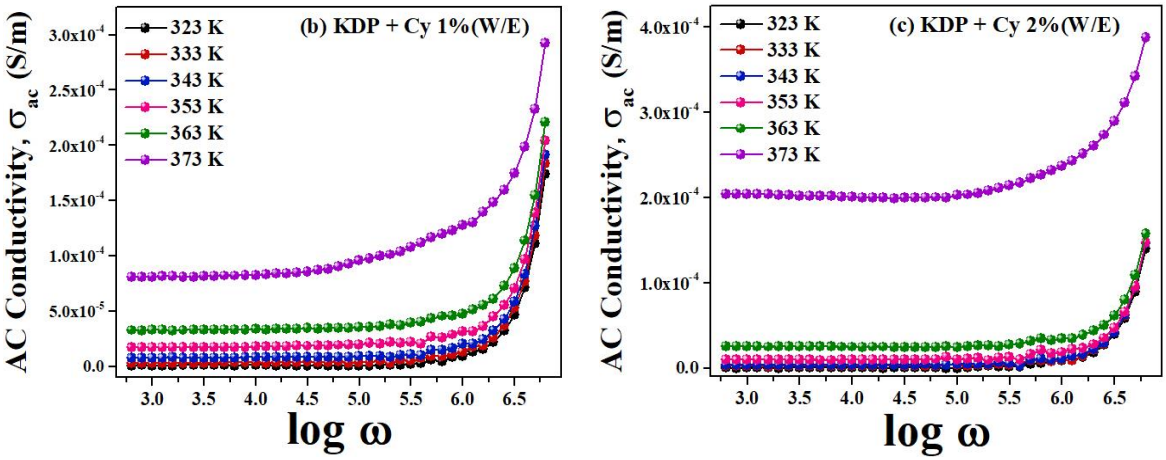

Figures 9. (b) A. C Conductivity of L-Cysteine (1 mol%) doped KDP crystals and **(c)** A. C Conductivity of L-Cysteine (2 mol%) doped KDP crystals

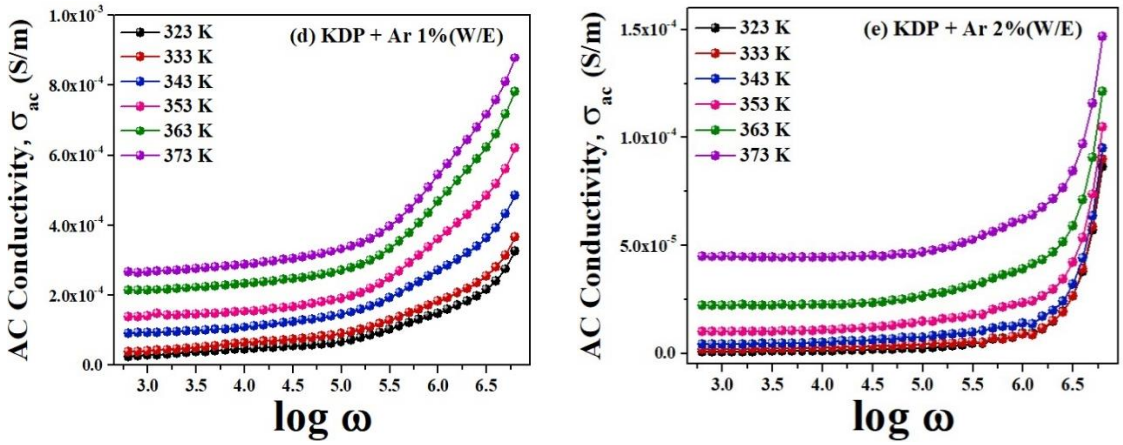

Figures 9. (d) A. C Conductivity of L-Arginine (1 mol%) doped KDP crystals and **(e)** A. C Conductivity of L-Arginine (2 mol%) doped KDP crystals

It is observed that the values of a. c conductivity of pure KDP and L-Arginine doped KDP crystals grown in the presence of an electric field are more than those of pure KDP and L-Arginine doped KDP crystals grown in the absence of an electric field (Chapter-4). Conductivity is caused by vacancies and weakly attached impurities in the crystal lattice at low temperatures. The increase in a. c conductivity with frequency is already discussed elaborately in Chapter-4.

3.2.3 Jonscher's Plots:

Jonscher plots for pure, L-Cysteine and L-Arginine doped KDP crystals (grown in the presence of an electric field) are shown in figures 10 (a-e), which reveal significant dispersive behaviour due to the presence of just a. c conductivity. A detailed description of Jonscher power is already given in Chapters-4 and 5. As seen in table 5, d. c conductivity increases with increasing temperature and dopant concentration. Table 6 represents the values of constant 'A'. Table 7 shows that for pure, L-Cysteine and L-Arginine (1 mol% and 2 mol%) doped KDP crystals, the 's' parameter value drops linearly with temperature, implying a Correlation Barrier Hopping (CBH) conduction mechanism [23]. As a result, the CBH model predicts that the most likely conduction mechanism in the crystals is the typical hopping of charge carriers between localized sites across the potential barrier.

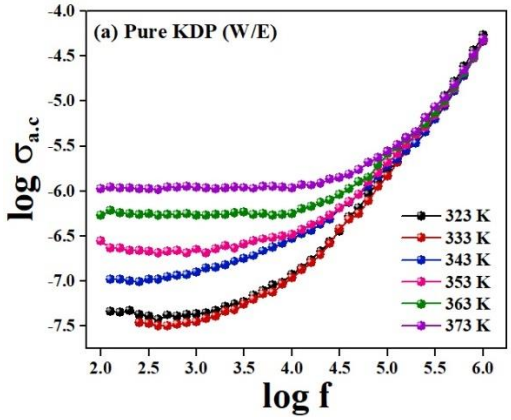

Figure 10(a). Jonscher's plot of pure KDP crystal

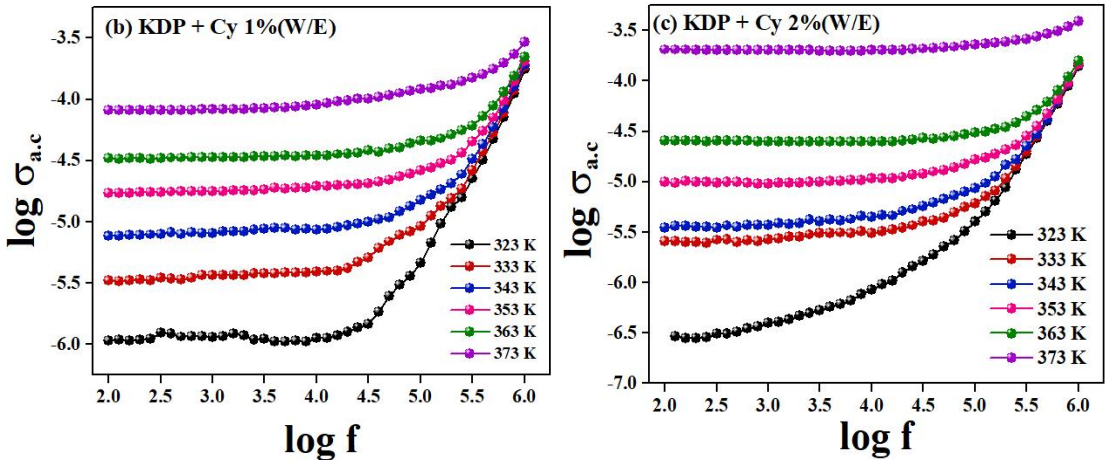

Figures 10. (b) Jonscher's plot of L-Cysteine (1 mol%) doped KDP crystals and **(c)** Jonscher's plot of L-Cysteine (2 mol%) doped KDP crystals

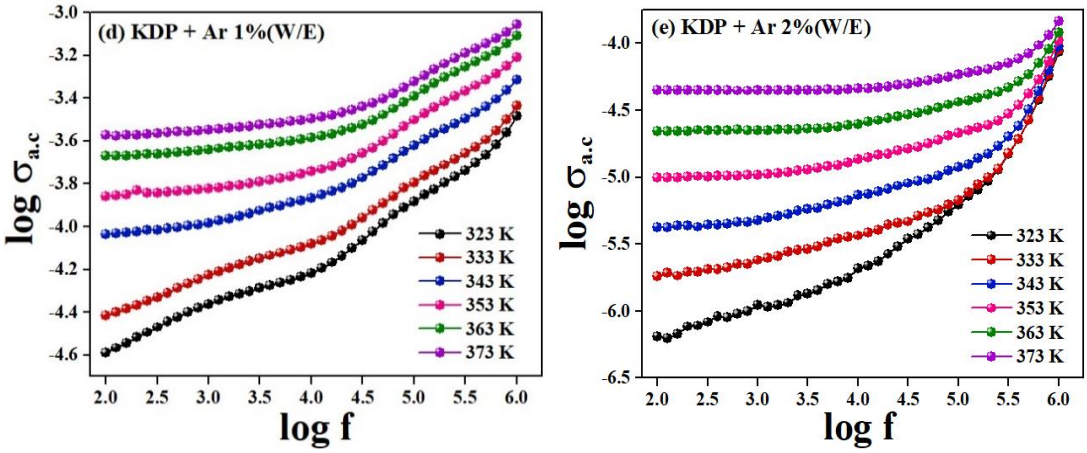

Figures 10. (d) Jonscher's plot of L-Arginine (1 mol%) doped KDP crystals and **(e)** Jonscher's plot of L-Arginine (2 mol%) doped KDP crystals

Table 5. $\sigma_{d.c}$ conductivity values of pure, L-Cysteine (1 mol% and 2 mol%) and L-Arginine (1 mol% and 2 mol%) doped KDP crystals

Temperature	$\sigma_{d.c}$ conductivity				
	Pure KDP (W/E)	**KDP + Cy 1% (W/E)**	**KDP + Cy 2% (W/E)**	**KDP + Ar 1% (W/E)**	**KDP + Ar 2% (W/E)**
323 K	2.98×10^{-8}	1.08×10^{-6}	0.3×10^{-6}	2.537×10^{-5}	0.7138×10^{-6}
333 K	3.12×10^{-8}	3.3×10^{-6}	2.513×10^{-6}	3.741×10^{-5}	1.824×10^{-6}
343 K	1.0157×10^{-7}	7.652×10^{-6}	3.514×10^{-6}	9.1×10^{-5}	4.1863×10^{-6}
353 K	2.247×10^{-7}	1.725×10^{-5}	9.627×10^{-6}	1.409×10^{-4}	9.7214×10^{-6}
363 K	5.525×10^{-7}	3.314×10^{-5}	2.5036×10^{-5}	2.105×10^{-4}	2.15×10^{-5}
373 K	1.025×10^{-6}	8.08×10^{-5}	1.981×10^{-4}	2.6×10^{-4}	4.45×10^{-5}

Table 6. Values of Jonscher's plot parameter 'A' of pure, L-Cysteine (1 mol% and 2 mol%) and L-Arginine (1 mol% and 2 mol%) doped KDP crystals

Temperature	A ($s.m^{-1}.rad^{-n}$)				
	Pure KDP (W/E)	**KDP + Cy 1% (W/E)**	**KDP + Cy 2% (W/E)**	**KDP + Ar 1% (W/E)**	**KDP + Ar 2% (W/E)**
323 K	1.541×10^{-11}	1.041×10^{-10}	1.025×10^{-10}	8.24×10^{-8}	5.17×10^{-9}
333 K	1.952×10^{-11}	1.817×10^{-10}	1.4×10^{-10}	9.836×10^{-8}	6.074×10^{-9}
343 K	2.284×10^{-11}	4.935×10^{-10}	1.831×10^{-10}	2.541×10^{-7}	8.517×10^{-9}
353 K	2.3896×10^{-11}	8.152×10^{-10}	2.115×10^{-10}	2.841×10^{-7}	1.524×10^{-8}
363 K	2.788×10^{-11}	9.521×10^{-10}	2.382×10^{-10}	3.6×10^{-7}	1.827×10^{-8}
373 K	3.284×10^{-11}	2.541×10^{-9}	1.25×10^{-9}	4.27×10^{-7}	2.105×10^{-8}

Different formulae (Ref. Chapter 4) were used to compute the crystals' binding energy (Wm), the activation energy, and the density of states at the Fermi level. The binding energy W_m was estimated using the slope of the linear plot of 1-s versus T. The variation in 1-s with temperature for pure, L-Cysteine (1 mol% and 2 mol%) and L-Arginine (1 mol% and 2 mol%) doped KDP crystals is shown in figure 11.

Table 7. Value of Jonscher's plot parameter 's' of pure, L-Cysteine (1 mol% and 2 mol%) and L-Arginine (1 mol% and 2 mol%) doped KDP crystals

Temperature	s - parameter				
	Pure KDP (W/E)	KDP + Cy 1% (W/E)	KDP + Cy 2% (W/E)	KDP + Ar 1% (W/E)	KDP + Ar 2% (W/E)
323 K	0.9719	0.9263	0.9362	0.5913	0.6024
333 K	0.9683	0.915	0.9169	0.5841	0.5901
343 K	0.9642	0.8394	0.9043	0.5508	0.5873
353 K	0.9587	0.8306	0.8872	0.5427	0.5814
363 K	0.9504	0.8136	0.8631	0.5351	0.5768
373 K	0.9482	0.8061	0.8593	0.5250	0.568

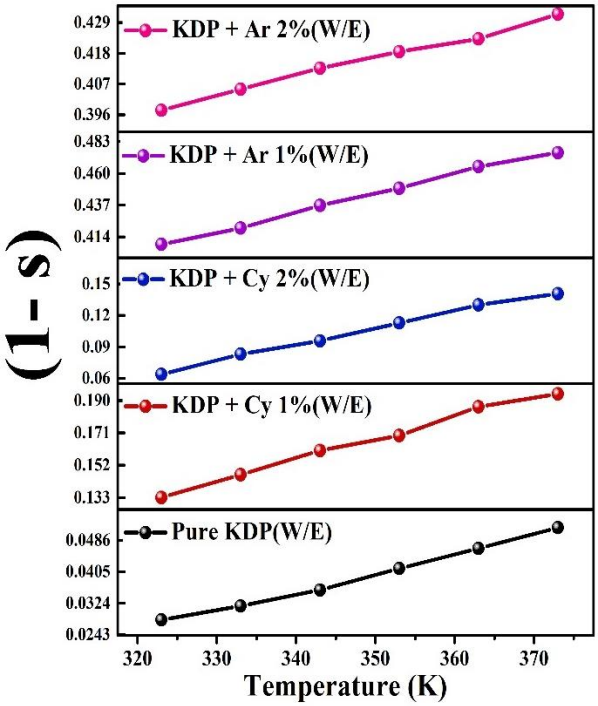

Figure 11. Binding energy plot of pure, L-Cysteine (1 mol% and 2 mol%) and L-Arginine (1 mol% and 2 mol%) doped KDP crystals

The binding energies of pure KDP, L-Cysteine (1 mol%) doped KDP, L-Cysteine (2 mol%) doped KDP, L-Arginine (1 mol%) doped KDP and L-Arginine (2 mol%) doped KDP crystal is found to be 1.0752 eV, 0.4169 eV, 0.3335 eV, 0.380 eV and 0.7803 eV, respectively.

Figures 12(a-e) depict the variation of density of states at the Fermi level $[N(E_f)]$ with frequency. With increasing frequency, the density of states $[N(E_f)]$ of pure KDP and L-Cysteine and L-Arginine doped KDP crystals decreases. For a given temperature range, the

value of $N(E_f)$ initially drops to a minimum, which complies with the dielectric constant and a. c conductivity values. As a result, at low frequencies, both frequency and temperature affect the electrical conductivity. On the other hand, thermal agitation at higher frequencies is responsible for transporting charge carriers at localized sites. Here, the large values of $N(E_f)$ ($\sim 10^{40}$-10^{41}) implies that the charge transport in present crystals is dominated by hopping between pairs of sites.

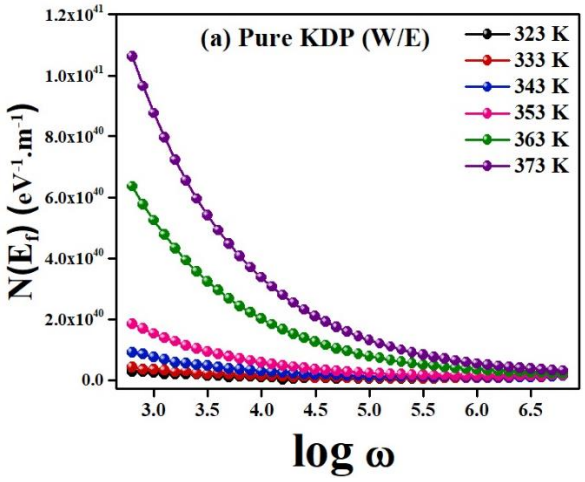

Figure 12(a). The variation of density of states at the Fermi level with frequency for pure KDP crystal

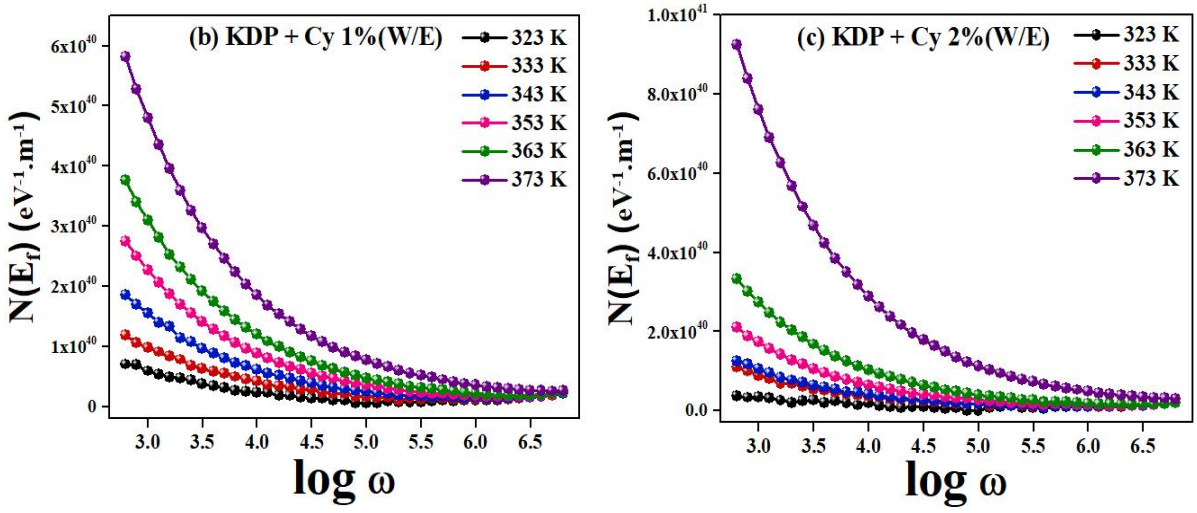

Figures 12. (b) The variation of density of states at the Fermi level with frequency for L-Cysteine (1 mol%) doped KDP crystal and **(c)** The variation of density of states at the Fermi level with frequency for L-Cysteine (2 mol%) doped KDP crystal

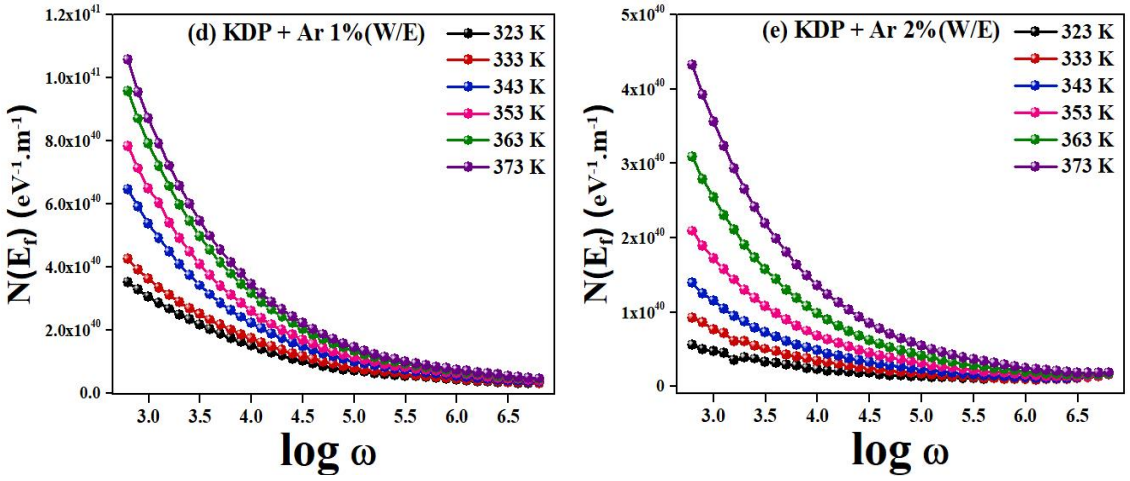

Figures 12. (d) The variation of density of states at the Fermi level with frequency for L-Arginine (1 mol%) doped KDP crystal and **(e)** The variation of density of states at the Fermi level with frequency for L-Arginine (2 mol%) doped KDP crystal

The log $_{a.c}$ versus 1000/T variation for pure, L-Cysteine and L-Arginine doped KDP crystals at various frequencies is shown in figures 13(a-e). The activation energies of pure, L-Cysteine and L-Arginine doped KDP crystals are calculated using the slopes of linear fitted log $\sigma_{a.c}$ vs. 1000/T. Table 8 shows the activation energies obtained at various frequencies. The activation energies of pure KDP, L-Cysteine and L-Arginine doped KDP crystals are seen to decrease as the frequency increases, implying that electronic charge carriers may hop between different localized states in the material [24].

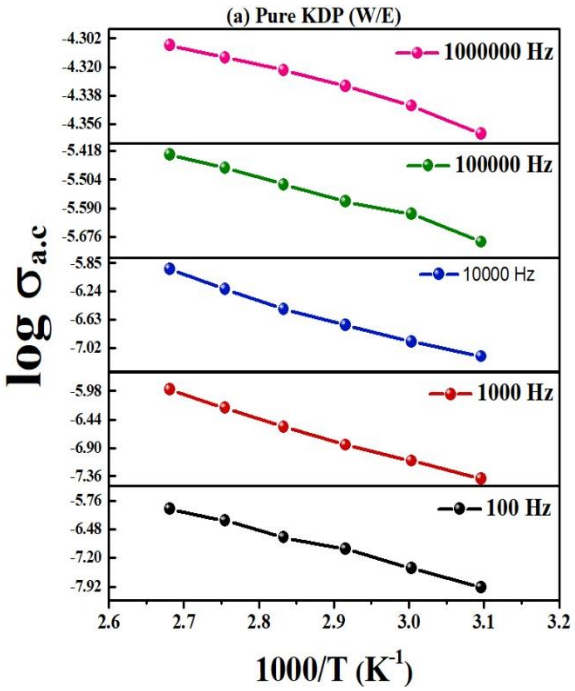

Figure 13(a). Activation energies plot for pure KDP crystal at different frequencies

Table 8. The calculated values of activation energies of pure, L-Cysteine and L-Arginine doped KDP crystals

Frequency (Hz)	Activation Energy (E_a) (eV)				
	Pure KDP (W/E)	KDP + Cy 1% (W/E)	KDP + Cy 2% (W/E)	KDP + Ar 1% (W/E)	KDP + Ar 2% (W/E)
100	0.9106	0.8574	1.2189	0.4841	0.8508
1000	0.6658	0.8462	1.0919	0.3887	0.7448
10000	0.5547	0.8338	0.9222	0.3455	0.6216
100000	0.1180	0.6190	0.4610	0.2743	0.4411
1000000	0.0253	0.0624	0.0320	0.2100	0.0825

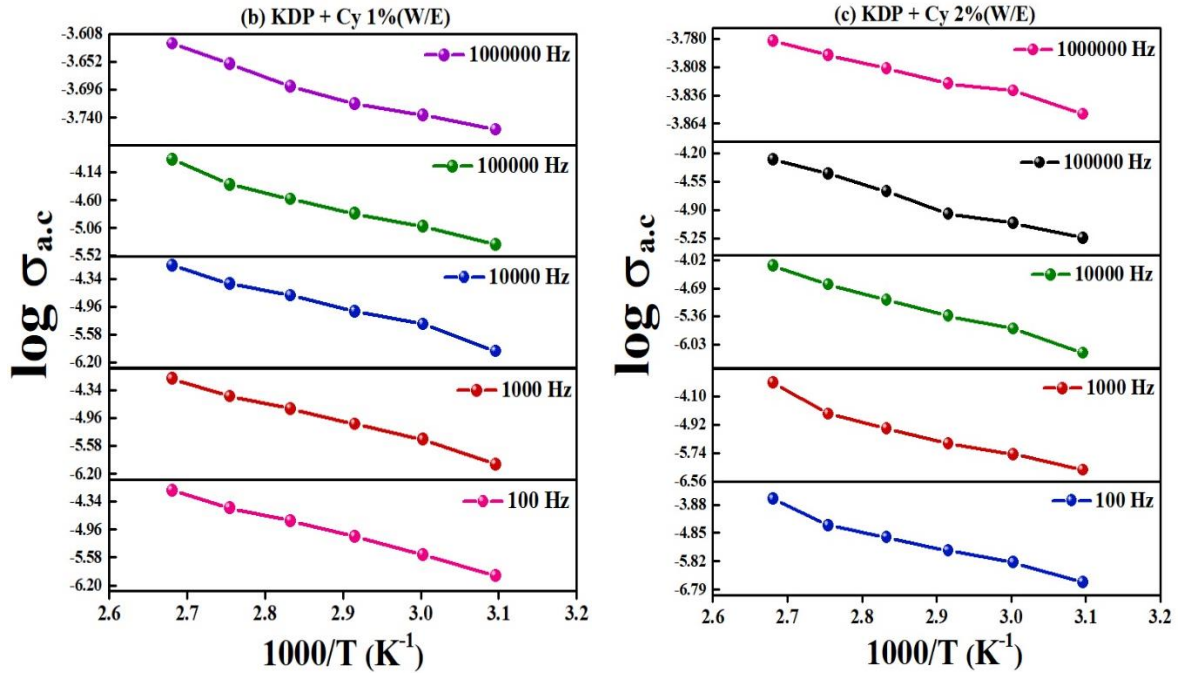

Figures 13. (b) Activation energies plots for L-Cysteine (1 mol%) doped KDP crystals at different frequencies and **(c)** Activation energies plots for L-Cysteine (2 mol%) doped KDP crystals at different frequencies

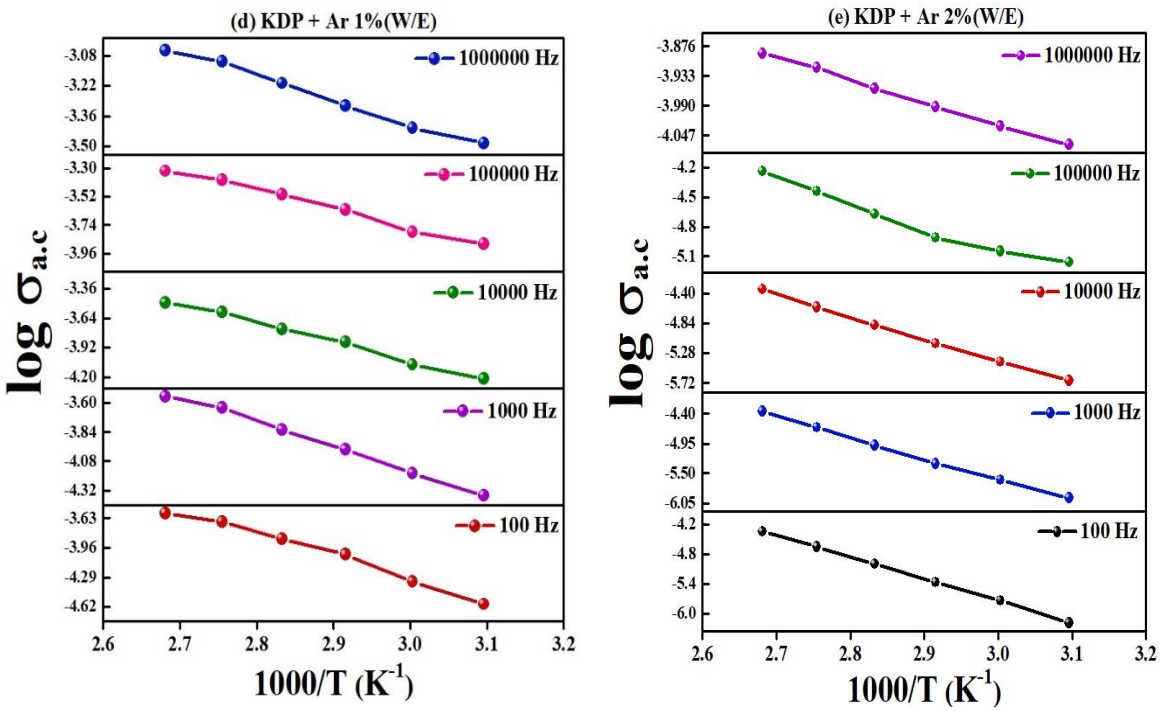

Figures 13. (d) Activation energies plots for L-Arginine (1 mol%) doped KDP crystals at different frequencies and **(e)** Activation energies plots for L-Arginine (2 mol%) doped KDP crystals at different frequencies

1.2.4 Complex Modulus Spectroscopy:

The plots in figures 14(a-e) show the relationship between the imaginary portion of the complex modulus (M'') and the real component of the complex modulus (M') at temperatures ranging from 323 to 373 K. All crystals whose centres do not lie on the real axis are shown by a single semi-circle in the figures, implying non-Debye type relaxation in the crystals. Using complex modulus spectroscopy, the electrode polarization and grain boundary conduction processes involved in the electrical relaxation can be distinguished.

The real part (M') and imaginary part (M'') of the complex modulus vary with angular frequency at temperatures ranging from 323 K to 373 K, as shown in figures 15(a-e) and 16(a-e). It is observed that M' has a lower magnitude at lower frequencies and demonstrates continuous dispersion as frequency increases. The maxima peaks M''_{max} move toward the high-frequency side as the temperature increases. Due to the long-range mobility of charge carriers under the action of an induced electric field, a sigmoidal reduction in the value M' of is observed with increasing frequency at all of the given temperatures. The frequency range below the

relaxation peak in the imaginary part of the modulus M'' defines the zone where the carrier can migrate over long distances.

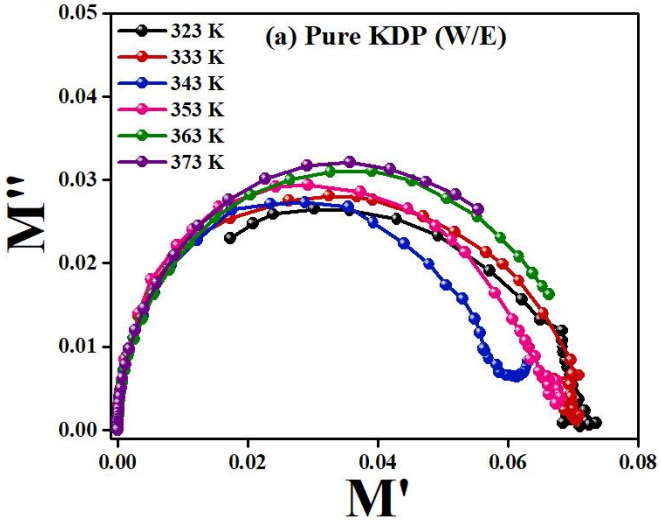

Figure 14(a). Variation in real (M') and imaginary (M'') parts of complex modulus for pure KDP crystal

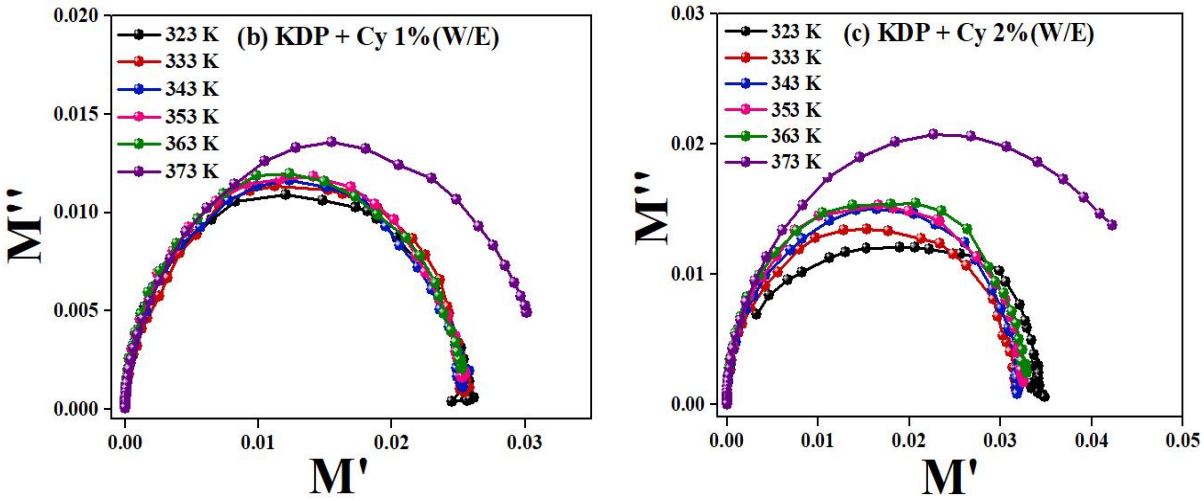

Figures 14. (b) Variation in real (M') and imaginary (M'') parts of complex modulus for L-Cysteine (1 mol%) doped KDP crystals and **(c)** Variation in real (M') and imaginary(M'') parts of complex modulus for L-Cysteine (2 mol%) doped KDP crystals

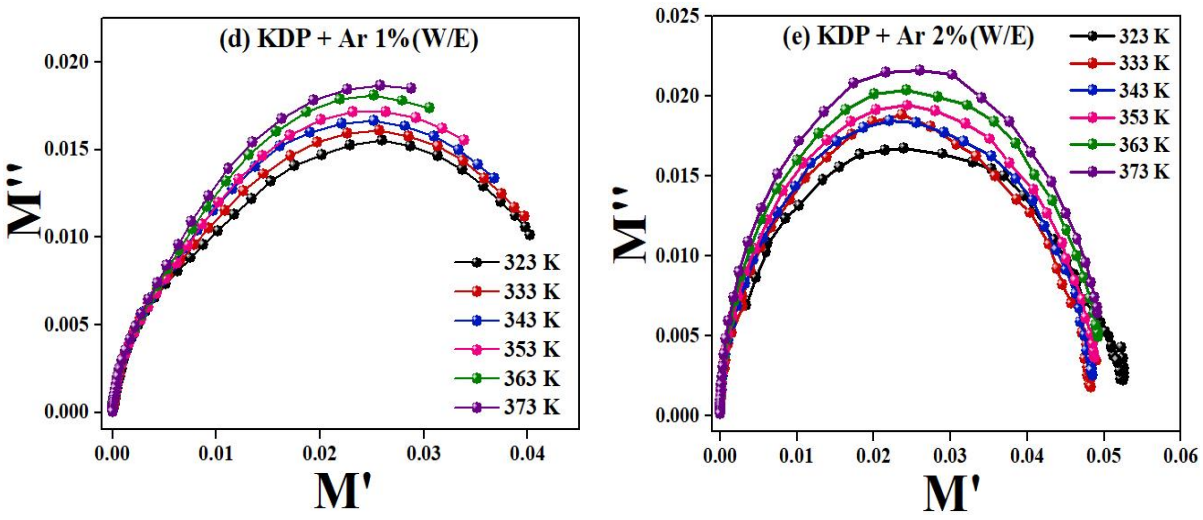

Figures 14. (b) Variation in real (M') and imaginary (M'') parts of complex modulus for L-Arginine (1 mol%) doped KDP crystals and **(c)** Variation in real (M') and imaginary(M'') parts of complex modulus for L-Arginine (2 mol%) doped KDP crystals

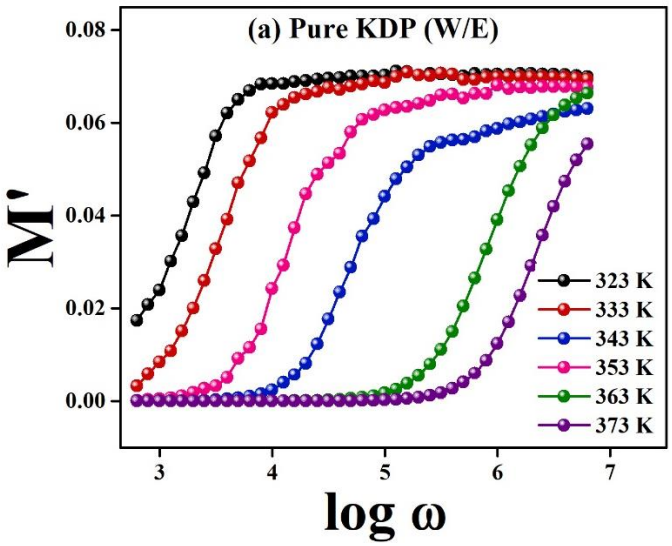

Figure 15(a). Variation of the real part of complex modulus (M') with angular frequency for pure KDP crystal

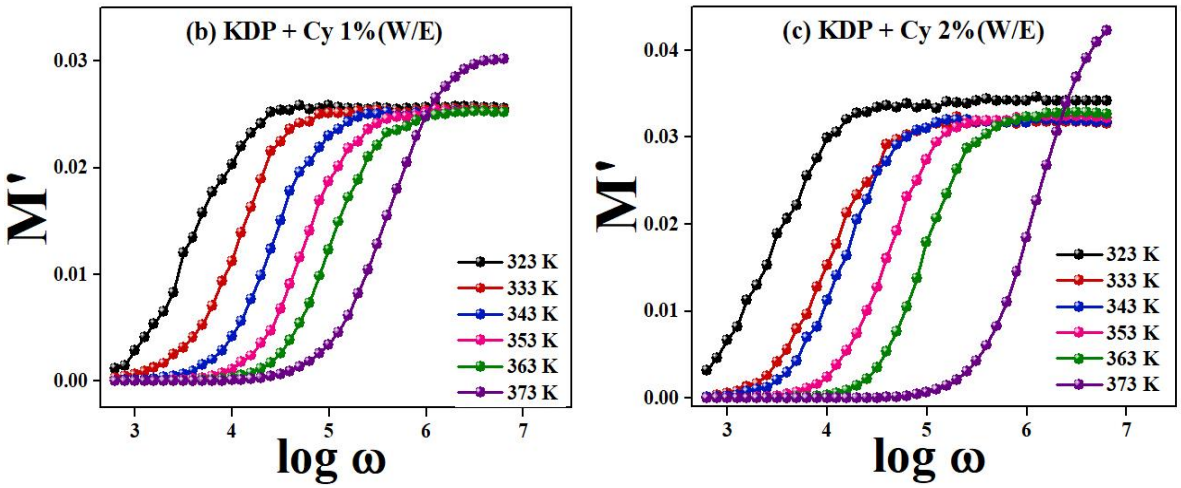

Figures 15. (b) Variation of the real part of complex modulus (M') with angular frequency for L-Cysteine (1 mol%) KDP crystal and **(c)** Variation of the real part of complex modulus (M') with angular frequency for L-Cysteine (2 mol%) KDP crystal

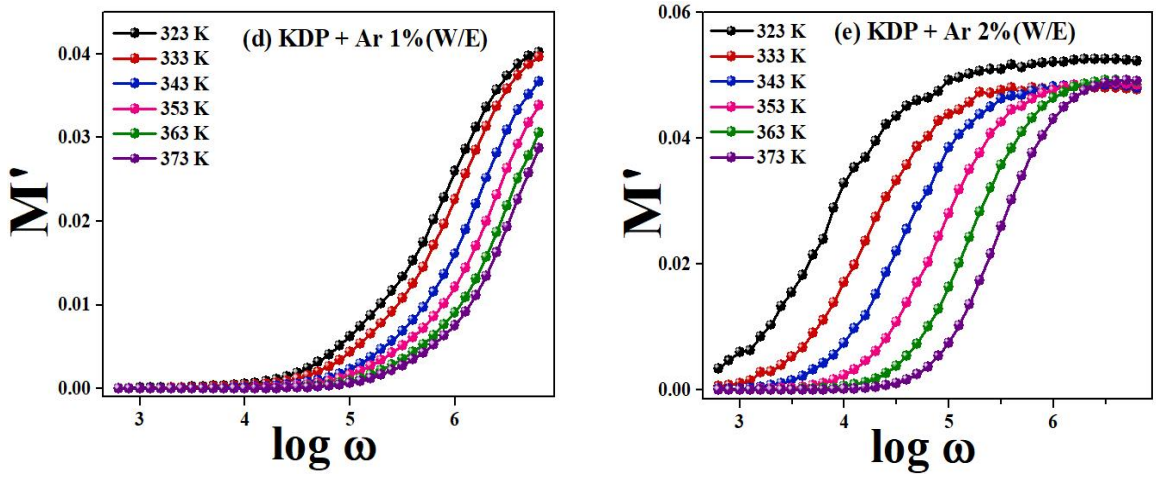

Figures 15. (d) Variation of the real part of complex modulus (M') with angular frequency for L-Arginine (1 mol%) KDP crystal and **(e)** Variation of the real part of complex modulus (M') with angular frequency for L-Arginine (2 mol%) KDP crystal

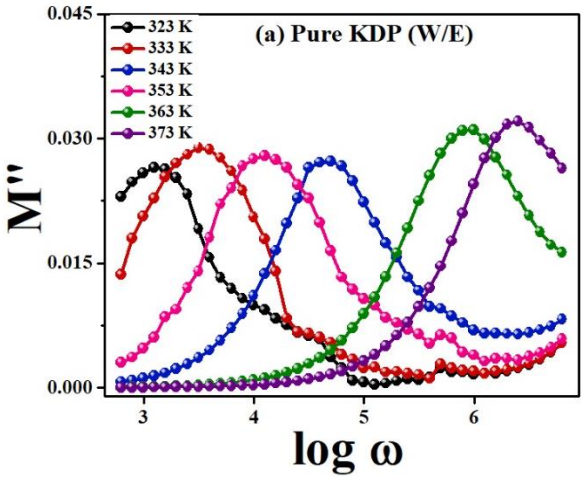

Figure 16(a). Variation of the imaginary part of complex modulus with angular frequency for pure KDP crystal

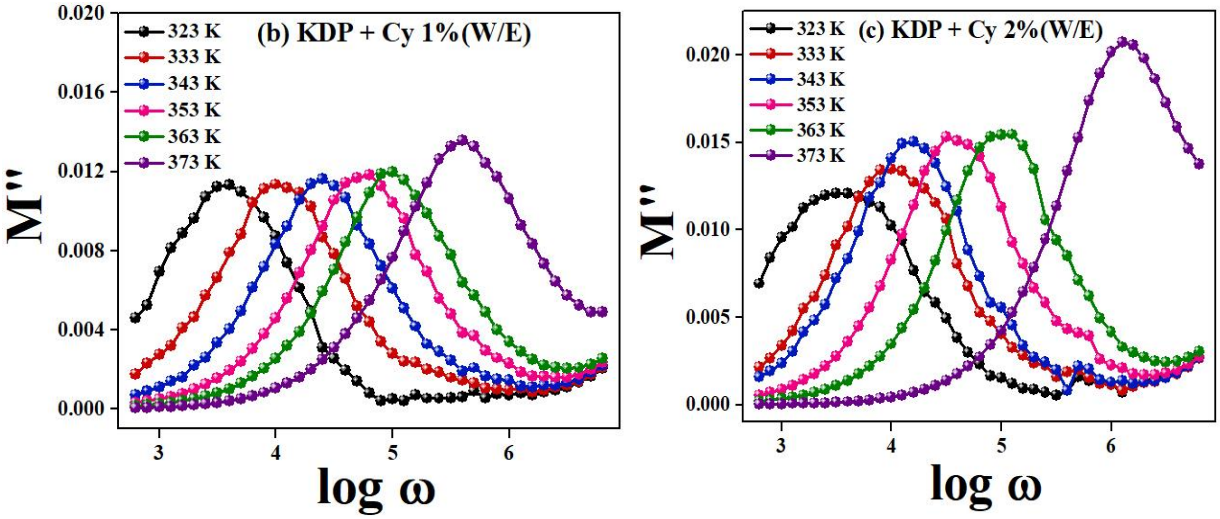

Figures 16. (b) Variation of the imaginary part of complex modulus with angular frequency for L-Cysteine (1 mol%) doped KDP crystals and **(c)** Variation of the imaginary part of complex modulus with angular frequency for L-Cysteine (2 mol%) doped KDP crystals

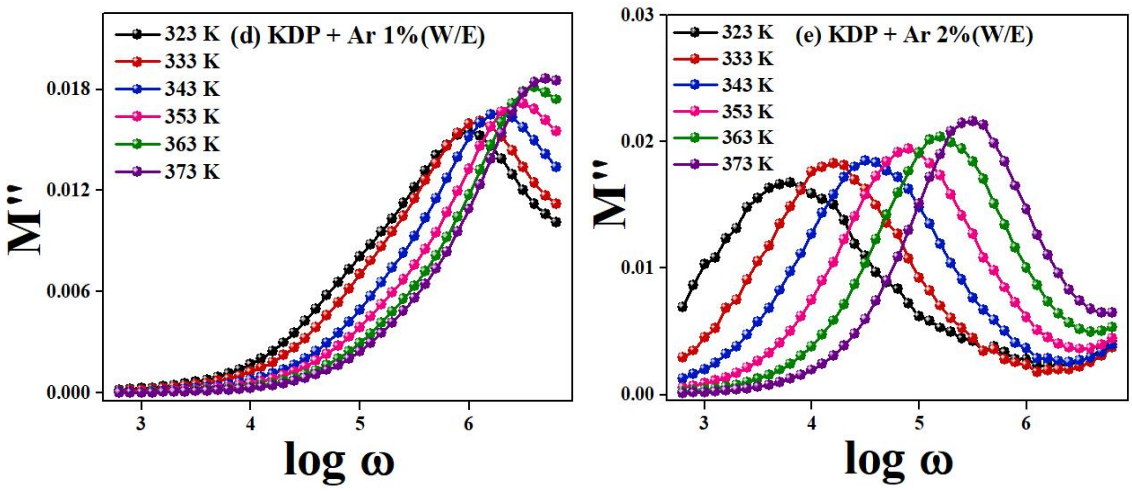

Figures 16. (d) Variation of the imaginary part of complex modulus with angular frequency for L-Arginine (1 mol%) doped KDP crystals and **(e)** Variation of the imaginary part of complex modulus with angular frequency for L-Arginine (2 mol%) doped KDP crystals

The modulus spectrum reveals that a hopping process arises due to the difference in a number of charge carriers, contributing greatly to electrical conductivity at high temperatures. At each temperature, at least one relaxation peak has been observed. The stretch exponent parameter (β) was determined and is reported in table 9 using relaxation peaks at various temperatures. The value of β deviates from unity in pure, L-Cysteine and L-Arginine doped KDP crystals, implying a non-Debye type relaxation mechanism.

Table 9. The calculated values of stretch exponent parameter (β) for pure KDP, L-Cysteine and L-Arginine doped KDP crystals

Temperature	Stretch exponent parameter (β)				
	Pure KDP (W/E)	KDP + Cy 1% (W/E)	KDP + Cy 2% (W/E)	KDP + Ar 1% (W/E)	KDP + Ar 2% (W/E)
323	0.8465	0.9411	0.7636	0.5208	0.6827
333	0.9074	0.9698	0.9042	0.5503	0.7724
343	0.9241	0.9854	0.9618	0.5652	0.7792
353	0.9651	0.9576	0.9495	0.5306	0.7694
363	0.7555	0.9138	0.9231	0.5131	0.7302
373	0.7942	0.7215	0.7421	0.4980	0.7467

3.3 Fourier Transform Infrared (FT-IR) Spectroscopy:

The FTIR spectra of pure and doped KDP crystals grown in an electric field are shown in figures 17(a-e). Because of the strain in the lattice caused by the dopant, some of the vibrational frequencies have shifted significantly. Table 10 lists the functional groups as well as various vibrational frequencies. Different amino acid functional groups overlap with those of KDP. In the region 2700-3300 cm^{-1}, asymmetric stretching vibrations of NH^{3+} of amino acid overlap with OH stretching vibration of KDP. The unification of dopants in KDP is revealed by the functional groups of amino acids found in doped KDP crystals [25].

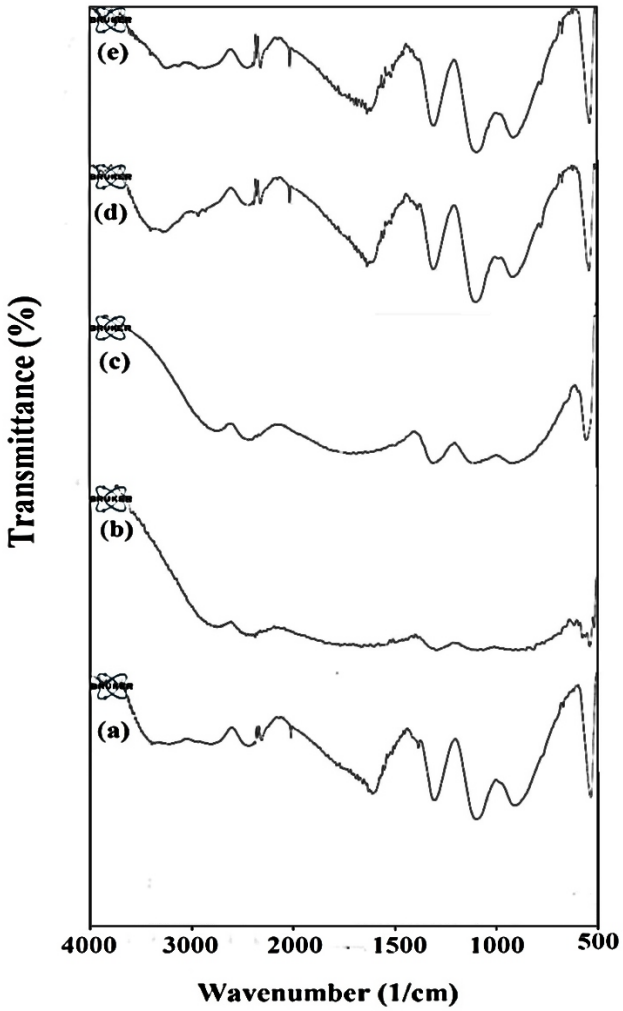

Figure 17. FTIR spectra of Pure KDP and doped KDP crystals grown in the presence of an electric field **(a)** Pure KDP crystal, **(b)** L-Cysteine (1 mol%) doped KDP crystal, **(c)** L-Cysteine (2 mol%) doped KDP crystal, **(d)** L-Arginine (1 mol%) doped KDP and **(e)** L-Arginine (2 mol%) doped KDP crystal

Table 10. List of various functional groups of pure and doped KDP crystals.

Bond Assignments	Wavenumber (cm^{-1})				
	Pure KDP W/E	**KDP + Cy1% (W/E)**	**KDP + Cy2% (W/E)**	**KDP + Ar1% (W/E)**	**KDP + Ar2% (W/E)**
O-H vibration	3320	3324	3321	3336	3382
N-H stretching	-	2920	2921	2924	2925
O-H asymmetric stretching	2920	2923	2921	2924	2920
O-P-OH symmetric stretching	1703	1659	1683	1689	1678
O=P-OH stretching	1658	1659	1656	1657	1658
NH_3 bending	-	1454	1451	1453	1454
C-COO^- symmetric stretching	-	1415	1414	1416	1416
C=S symmetric stretching	-	717	716	-	-
C-N-H stretching	-	1291	1302	1304	1304
P=O stretching/ C-N stretching	1099	1087	1108	1094	1090
P-O-H stretching	909	989	985	983	986
NO_3 stretching	-	775	773	774	774
COOH rocking	-	668	667	669	668
COO^- bending	-	613-677	613-675	616-676	617-677
HO-P-OH bending/CH_2-CH-N bending	534	538	549	535	533

From the FTIR spectra of doped KDP crystals, it is observed that the absorption bands of KDP have shifted slightly. The FTIR spectra of L-Cysteine and L-Arginine doped KDP crystals reveal the symmetric stretching of C-H, C=O, and COOH groups. The dopants L-Arginine and L-Cysteine are expected to form L-defects by combining an unoccupied H-vacancy with the hydrogen atom of KDP. As a result of this, the basic vibration of hydrogen (OH vibration) is rehabilitated. We have calculated the force constant of O–H vibration for pure and doped KDP crystals using the formula described in Chapter-4. Table 11 shows the computed values of the force constant for OH vibration. It is observed that the force constant is changed due to the addition of L-Cysteine and L-Arginine.

Table 11. The calculated values of Force Constant of O-H vibration for pure and L-Cysteine and L-Arginine doped KDP crystals

Sample	Absorption Wavenumber (cm^{-1})	Force Constant (Nm^{-1})
Pure KDP (W/E)	3320	590.79
KDP + Cy 1% (W/E)	3395	617.78
KDP + Cy 2% (W/E)	3383	613.42
KDP + Ar 1% (W/E)	3397	618.51
KDP + Ar 2% (W/E)	3382	613.06

3.4 Ultraviolet-Visible (UV-Vis) Spectroscopy:

The pure and doped KDP crystals were found to be highly transparent between 350-800 nm. This wide spectral transparency lends credence to its use in optical applications. Figures 18(a-b) show the absorbance spectra of pure and doped KDP crystals. The formulae for optical absorption coefficient (α) and optical energy band gap have been discussed in Chapter-4. Figure 18(a) shows that the cut-off wavelengths of pure KDP and L-Cysteine (1 mol% and 2 mol%) doped KDP crystals are 250 nm, 248 nm and 247 nm, respectively. The cut-off wavelengths of L-Arginine (1 mol% and 2 mol%) are 244 nm and 242 nm, as observed in figure 18 (b).

The optical bandgap was determined by plotting $(\alpha h\upsilon)^2$ against E, Tauc plot, for pure and doped KDP crystals. Extrapolation of the linear part on the high energy side of the spectrum was used to determine the optical band gaps of pure and doped KDP crystals. From figure 19(a), the band gaps of pure KDP and L-Cysteine (1 mol% and 2 mol%) doped KDP crystal grown in the presence of an electric field were found to be 3.70 eV, 4.03 eV and 4.05 eV, respectively. Also, the band gaps of L-Arginine (1 mol% and 2 mol%) doped crystals grown in an electric field were found to be 4.95 eV and 5.01 eV, as shown in figures 19(b).

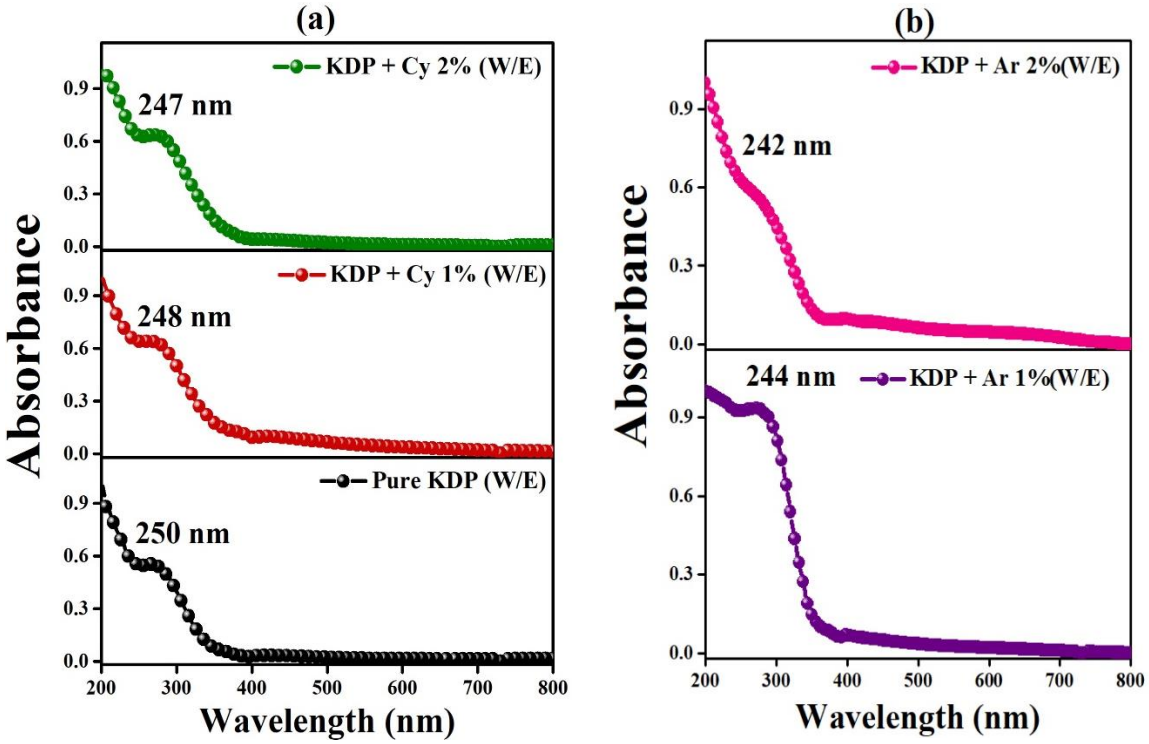

Figures 18. (a) Absorbance spectra for pure and L-Cysteine (1 mol% and 2 mol%) doped KDP crystals and **(b)** L-Arginine (1 mol% and 2 mol%) doped KDP crystals

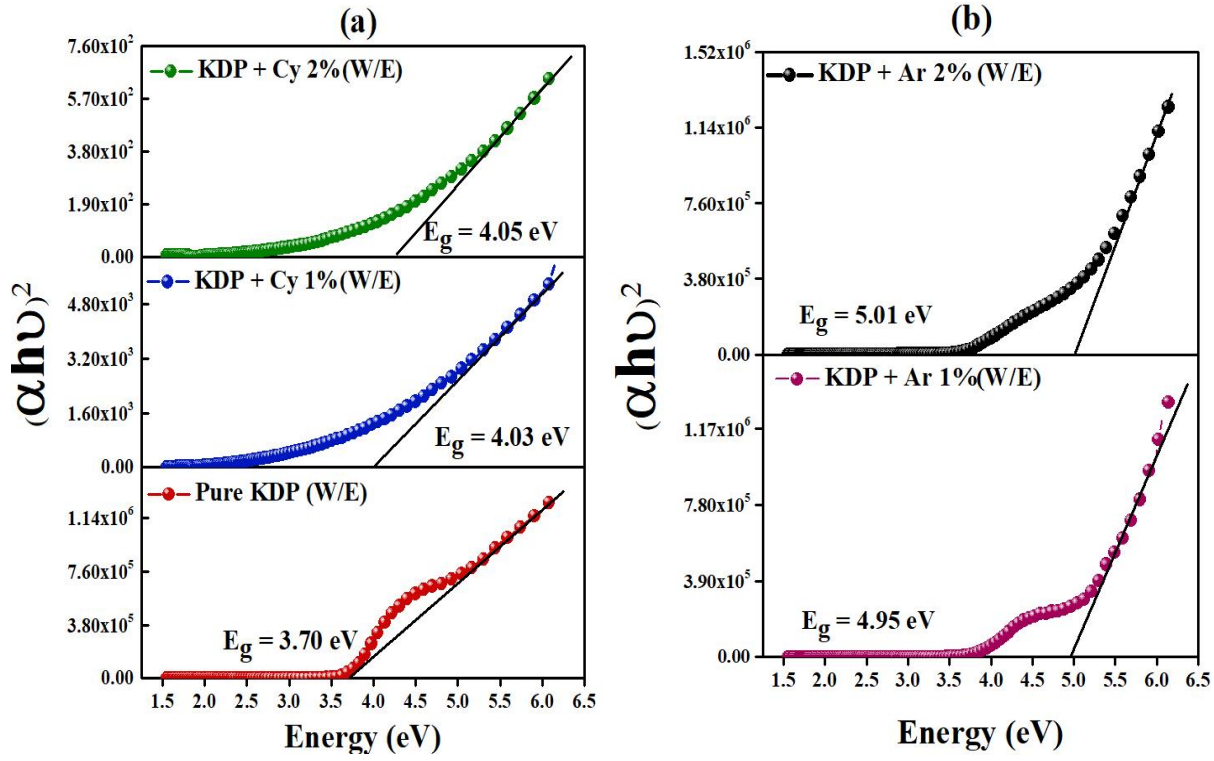

Figures 19. (a) Tauc's plot of pure and L-Cysteine (1 mol% and 2 mol%) doped KDP crystals and **(b)** Tauc's plot of L-Arginine (1 mol% and 2 mol%) doped KDP crystals

With the increase in doping percentage, there is an enhancement in the bandgap of doped crystals, and this notable increase in the bandgap of pure KDP due to amino acid doping prompts the possibility of increased SHG (Second Harmonic Generation) efficiency.

3.4.1 Urbach Energy (Absorption band tail):

The Urbach empirical rule (Ref. Chapter-4) at the optical bandgap edge describes the relationship between absorption coefficient and photon energy. The Urbach Energy (E_u) was calculated using the straight-line slope of ln (α) versus photon energy plots shown in figures 20(a-b), and the values obtained are shown in table 12.

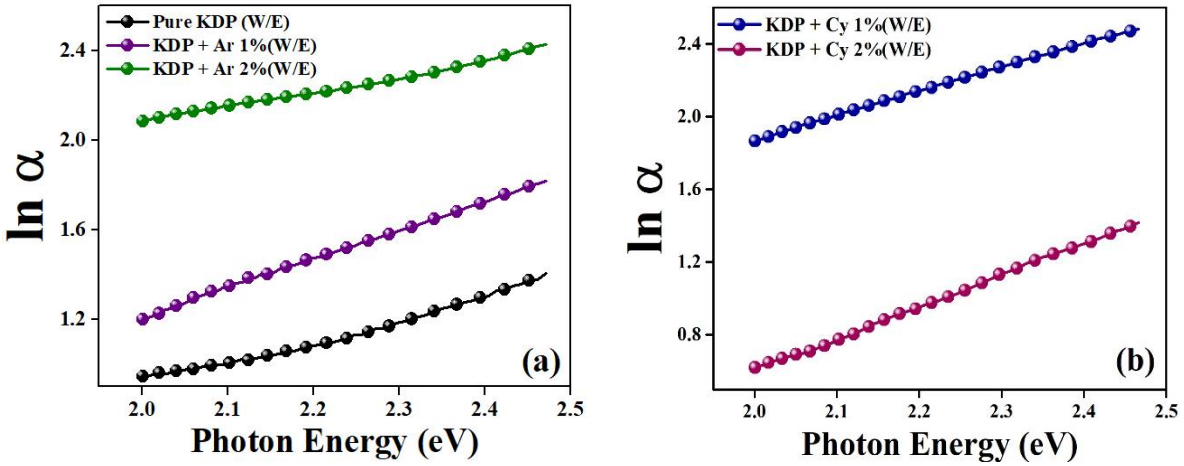

Figures 20. (a) Urbach energy plot for pure and L-Arginine (1 mol% and 2 mol%) doped KDP crystals and **(b)** Urbach energy plot for L-Cysteine (1 mol% and 2 mol%) doped KDP crystals

Table 12. The calculated values of Urbach energy (E_u) for pure, L-Cysteine and L-Arginine doped KDP crystals

Sample	Urbach Energy (E_u) (eV)
Pure KDP (W/E)	1.0460
KDP + Cy 1%(W/E)	0.7564
KDP + Cy 2%(W/E)	0.5719
KDP + Ar 1%(W/E)	0.7791
KDP + Ar 2%(W/E)	0.6351

3.5 Photoluminescence (PL) Analysis:

The photoluminescence emission spectra, obtained with 247nm excitation wavelength, of pure and L-Cysteine and L-Arginine doped KDP crystals are shown in figure 21(a).

Recombination in electronic transitions is one of the optical processes studied using the absorbance of photoluminescence at a specific wavelength. As seen in the transparency region of the crystal, the excitation is caused by a hydrogen vacancy (L-defect) dependent core associated with a heterovalent impurity. The spectra reveal three distinct emission peaks at different wavelengths and are listed in table 13. It can be seen from figure 21 that when the concentration of L-Cysteine amino acid increases, the intensity of the PL emission spectra increases, indicating that the dopant L-Cysteine has been incorporated in the KDP crystal; however, the emission intensity of the peaks decreases in L-Arginine doped crystals due to a reduction in the number of recombination centres. The phenomenon shows that an increase in impurity concentration causes L and D type orientational defects in the vicinity of the impurity atoms to compensate for the excess charge.

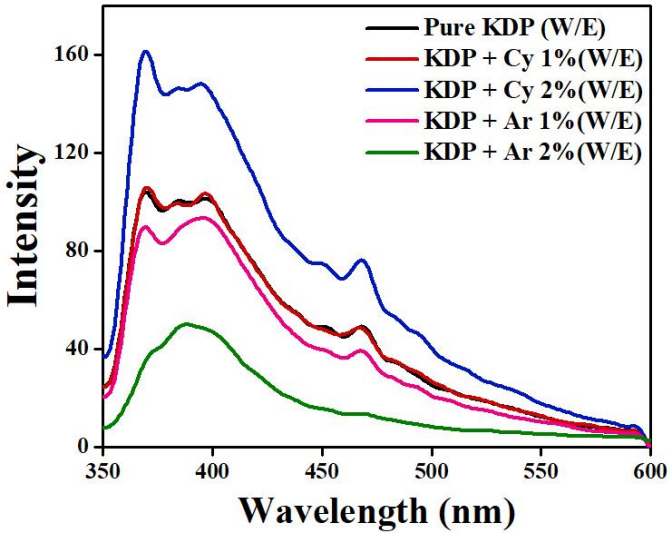

Figure 21(a). PL Emission spectra of pure and doped KDP crystals

Table 13. PL Emission peaks for pure and doped KDP crystals

Sample	Emission Wavelength (nm)	
Pure KDP	369.47	467.94
KDP + Cy 1%(W/E)	370.04	468.20
KDP + Cy 2%(W/E)	369.60	468.33
KDP + Ar 1%(W/E)	369.36	468.33
KDP + Ar 2%(W/E)	-	467.27

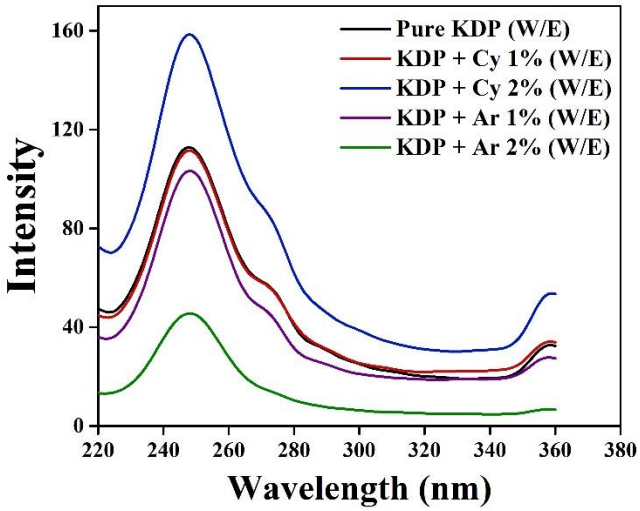

Figure 21(b). PL Excitation spectra of pure and doped KDP crystals

It is observed from table 14 that the Stoke shift increases as the doping concentrations of L-Arginine and L-Cysteine increase. This happens because L-Cysteine and L-Arginine have two charges, namely, NH^{3+} (positive) and COO^{-} (negative), forming a dipole there around while the KDP lattice surrounds it. When L-Cysteine and L-Arginine reach excited states under the influence of electromagnetic radiation, their dipole moments change, but the KDP lattice cannot adapt to it quickly enough. As a result, as the system vibrations relax, the dipole moments realign with the applied optical field. As the doping concentrations of L-Cysteine and L-Arginine are increased, it becomes difficult for KDP lattice to realign, due to which the Stokes shift in ascending order of doping increases.

Table 14. Variation in Stokes shift for pure and doped KDP crystals

Sample	Energy Absorption (eV)	Energy Emission (eV)	Stoke Shift (eV)
Pure KDP	4.9915	3.3523	1.6298
KDP + Cy 1%(W/E)	4.9965	3.3617	1.6439
KDP + Cy 2%(W/E)	5.0002	3.3563	1.6442
KDP + Ar 1%(W/E)	5.0009	3.3585	1.6424
KDP + Ar 2%(W/E)	5.0098	-	-

3.6 Relative Second Harmonic Generation (SHG) efficiency:

Table 15 shows the calculated values of relative SHG efficiency using the ratio of output power to input power. It is observed that the relative SHG efficiency of L-Arginine doped KDP crystals grown in the presence of an electric field has increased significantly. It can be plausibly explained that the molecular alignment of L-Arginine doped KDP crystals grown in the presence of an electric field increases nonlinearity, thereby increasing SHG efficiency. The weakening of the bonds between O-H and C=O (hydrogen bonding) may cause this increase in nonlinearity. Thus, the inclusion of L-Arginine molecules in the KDP crystal lattice, as well as additional hydrogen bonds created between atoms/molecules and preferential growth of the crystal along a particular axis, namely [001], may account for the substantial increase in SHG efficiency of doped KDP crystals [26]. As a result, L-Cysteine and L-Arginine doped KDP crystals grown in the presence of an electric field have a higher SHG efficiency than pure KDP crystals.

Table 15. Relative SHG efficiency of pure and doped KDP crystals

Sample	Relative SHG Efficiency
Pure KDP	-
KDP + Cy 1%(W/E)	2
KDP + Cy 2%(W/E)	2.5
KDP + Ar 1%(W/E)	3
KDP + Ar 2%(W/E)	5

4. Conclusion:

The pure and doped KDP crystals grown using the slow evaporation method have good quality and transparency. An elongation along the c-axis [100] was observed in L-Cysteine and L-Arginine doped KDP crystals. The impurity causes this elongation in crystals which are grown in the presence of an electric field. Powder XRD analysis verified crystalline perfection. No significant peak shifting indicates that the dopant L-Cysteine and L-Arginine atoms/molecules are satisfactorily accommodated in the KDP crystal structure. The formation of lattice defects is shown to increase the a. c conductivity of KDP crystals doped with the amino acids L-Cysteine and L-Arginine. Using Jonscher's power law, it was observed that pure, L-Cysteine, and L-Arginine doped KDP crystals follow the Correlation Barrier Hopping (CBH) conduction mechanism. The binding energy (W_m) and density of state at the Fermi level

[$N(E_f)$] were calculated. The a. c conductivity indicates a thermally induced mechanism for all the crystals under study. Based on complex impedance spectroscopy analysis, it is noted that even a small amount of L-Cysteine and L-Arginine doping in KDP crystal generates substantial changes in the bulk resistance and capacitance values, as well as the conduction mechanism. The Nyquist plots indicate one depressed semi-circle for all crystals studied, successfully represented by one R-CPE parallel circuit. The FTIR spectra show that the doped crystals contain the amino acid with an amine functional group. Based on the value of force constant measured for O–H vibration in doped KDP crystals, it is found that the L-Cysteine and L-Arginine atoms/molecules have not disrupted the lattice structure of KDP. Using the emission spectra of the crystals, the electronic transition resulting from light absorption by intrinsic impurities that generate colour-centre emissions can be investigated. The relative SHG efficiency of L-Arginine (2 mol%) doped KDP crystals grown in an electric field was found to be around 5 times that of pure KDP crystals. The high value of SHG efficiency suggests that crystals might be used in laser fusion and frequency conversion investigations.

References:

1. Z. Lin Z, Z. Wang, C. Chen, *J. Chem. Phys.*, **118** (2003) pp. 2349-2356.
2. N. Balamurugan, P. Ramasamy, *J. Cryst. Growth Des.*, **6** (2006) pp. 1642-1644.
3. A. Mahadik, P. H. Soni, C. F. Desai, *J. Physica B: Condensed Matt.*, **52** (2017) pp. 61-65.
4. K. Bouchouit, H. Bougharraf, B. Derkowska-Zielinska, N. Benali-Cherif, B. Sahraoui, J. *Opt. Mater.*, **48** (2015) pp. 215-221.
5. S. Sasi, R. Robert, S. Arumugam, C. Inmozhi, *J. Optik*, **127** (2016) pp. 2366-2369.
6. A. I. Ramakers Lennart, J. McGinty, W. Beckmann, G. Levilain, et al., *J. Cryst. Growth Des.*, **20** (2020) pp. 4935-4944.
7. A. P. Voronov, V. I. Salo, V. M. Puzikov, V. F. Tkachenko, Y. T Vydai, *Crystallogr. Rep.*, **51**(4) (2006) pp. 696-701.
8. G.G. Muley, M.N. Rode, B.H. Pawar, *Acta Phys. Pol.*, **A116** (2009) pp. 1033-1038.
9. G. Deepa, T. H. Freeda, C. Mahadevan, *Indian J. Phys.*, **76**(A) (2002) 369.
10. M. S. Pandian, K. Boopathi, P. Ramasamy, G. Bhagavannarayana, *Mater. Res. Bull.*, **47** (2012) pp. 826-835.
11. J. Podder, S. Ramalingom, S. Narayana Kalkura, *Cryst. Res. Technol.*, **36** (2001) pp. 549-556.
12. R. Davey, *J. Cryst. Growth*, **34**(1) (1976) pp. 109–119.
13. L. A. Shuvalov, Modern Crystallography IV: Properties of Crystals, Springer, Berlin, 1988, pp. 178–185.
14. G. Shanmugam, K. Thirupugalmani, K. Rakhikrishna, J. Philip, S. Brahadeeswaran, *J. Therm. Anal. Calorim.*, **114** (2013) pp. 1245-1254.
15. M. Anis, G. G. Muley, G. Rabbani, M. D. Shirsat, S.S. Hussaini, *Mater. Technol. Advc. Perform. Mater.*, **30** (2015) pp. 129-133.
16. M. M. Costa, G. F. M. Pires, A. J. Terrozo, M. P. F. Graca, A. S. B. Somba, *J. Appl. Phys.*, **110** (2011) pp. 034107(1-7).
17. A. Holden, The Nature of Solids, Columbia University, New York, 1992.
18. J. B. Goodenough, J. Jensen, A. Potier, Solid State Protonic Conductors III, Odense University Press, Denmark, 1984.
19. S. Chandra, Superionic Solids Principles and Applications, North-Holland Publishing Co., Amsterdam, Oxford, New York, 1981.

20. L. B. Harris, G. J. Vella, *J. Chem. Phys.*, **58** (1973) pp. 4550-4557.

21. E. P. Lokshin, *Crystallogr. Rep*., **41** (1996) 1070.

22. M. Meena, C. K. Mahadevan, *Cryst. Res. Technol.*, **43** (2008) pp. 166-172.

23. S. Mollah, K. K. Som, B. K. Bose, J. Chaudhuri, *J. Appl. Phys.*, **74** (1993) pp. 931-937.

24. M. A. Afifi, A. E. Berkheet, E. Elwahabb, H. E. Atvia, *Vacuum*, **61**(1) (2001) pp. 9-17.

25. A. Mahadik, P.H. Soni, K. Chaudhari, AIP Conference Proceedings **2265** (2020) pp. 030421(1)-030421(4).

26. E.I. Kostenyukova, I.M. Pritula, O.N. Bezkrovnaya, N.O. Kovalenko, A. G. Doroshenko, S.V. Khimchenko, A.G. Fedorov, *Semiconductor Physics, Quantum Electronics and Optoelectronics* (SPQEO) **22**(1) (2019) pp. 60-66.